Jagiellonian University in Cracow

Faculty of Physics, Astronomy and Applied Computer Science

Ewelina Kubicz

Student number: 1051798

The impact of a patient's size on a spatial resolution of PET scanner constructed of polymer scintillators

Master Thesis

Major: Biophysics

Specialisation: Medical Physics

Supervised by

Prof. dr hab. Paweł Moskal

Institute of Physics

Division of Nuclear Physics

Kraków 2014

Oświadczenie autora pracy

Świadoma odpowiedzialności prawnej oświadczam, że niniejsza praca dyplomowa została napisana przeze mnie samodzielnie i nie zawiera treści uzyskanych w sposób niezgodny z obowiązującymi przepisami. Oświadczam również, że przedstawiona praca nie była wcześniej przedmiotem procedur związanych z uzyskaniem tytułu zawodowego w wyższej uczelni.

Kraków, dnia

Podpis autora pracy

Oświadczenie kierującego pracą

Potwierdzam, że niniejsza praca została przygotowana pod moim kierunkiem i kwalifikuje się do przedstawienia jej w postępowaniu o nadanie tytułu zawodowego.

Kraków, dnia

Podpis kierującego pracą

Acknowledgements

I would like to express my highest gratitude to all people without whom this thesis would not have been possible.

First of all I thank Prof. Paweł Moskal for valuable help, plenty of hints and suggestions and mostly for understanding and enormous patience.

I would like to offer my gratitude to Szymon Niedźwiecki for his enormous help and a lot of time spent explaining to me even the simplest things.

I also thank my colleagues: Neha G. Sharma and Natalia Zoń for the scientific contribution, every corrected "form" and the great time spend together.

Many thanks to Oleg, for your help, always interesting discussions and lot of time spent trying to prove me I'm not always right, but mostly for all corrections, done as it is usually with me, at the last minute.

I wish to thank all my friends for a lots of patient and support. Here I especially want to thank Marzena for always being able to find the right reasons for me to work whenever I was losing my motivation.

Dziękuję także moim Rodzicom za pomoc, wsparcie, ogrom cierpliwości, a przede wszystkim wyrozumiałość.

Abstract

The impact of a patient's size on a spatial resolution of PET scanner constructed of polymer scintillators

The aim of this thesis is to determine how size of a patient influences the temporal and spatial resolution of a double module of Strip PET prototype based on polymer scintillators. Such a scanner is currently being developed at Jagiellonian University by the J-PET collaboration. All measurements were conducted using a double module of a Strip PET prototype with a ^{22}Na source. Four different sizes of phantoms filled with water or ethyl alcohol were used as a simulation of a patient's body. The achieved time resolution along Line-of-Response is around 146 ps, and it is the same for all tested phantoms within the uncertainty range and as a result spatial resolution along Line-of-Response is equal to about 22 mm. Both these values are two times better than in currently used PET scanners.

Streszczenie

Wpływ rozmiarów pacjenta na rozdzielczość przestrzenną tomografu PET zbudowanego z paskowych scyntylatorów

Głównym celem tej pracy jest wyznaczenie wpływu rozmiarów pacjenta na czasową i przestrzenną rozdzielczość paskowego tomografu PET zbudowanego z polimerowych scyntylatorów. Taki właśnie skaner jest obecnie budowany na Uniwersytecie Jagiellońskim. Wszystkie pomiary zostały przeprowadzone na dwu-modułowym prototypie PET używając ^{22}Na jako źródła promieniotwórczego. Cztery różnej wielkości fantomy, wypełnione wodą lub alhololem zostały wykorzystane w ramach tej pracy. Otrzymana rozdzielczość pomiaru czasu przelotu wynosi około 146 ps. Wartość ta jest dla wszystkich fantomów taka sama w granicach niepewności pomiarowych. Wyznaczona rozdzielczość przestrzenna wzdłuż linii lotu kwantów anihilacyjnych wynosi około 22 mm i w granicach niepewności jest taka sama dla wszystkich fantomów. Uzyskane rozdzielczości są dwukrotnie lepsze niż w obecnie produkowanych tomografach.

Contents

1 Introduction

Nowadays Positron Emission Tomography is one of main diagnostic techniques used in medicine. PET is used for non-invasive imaging of physiological processes occurring in the human body. It is very precise tool not only for diagnostic, but also for monitoring effects of therapy in oncology, cardiology, neurology and even psychiatry. It is also used to monitor progresses of radiotherapy and also it allows for early detection of Huntington disease. Development of Positron Emission Tomography has allowed for better understanding of ethology and progress of Alzheimer's and Parkinson's diseases, as well as schizophrenia and epilepsy. Through PET, diagnosis of different types of cancer in early stages is possible.

Commercial PET scanners are constructed of inorganic scintillators as radiation detectors [2, 4, 8]. Because of that, these scanners are very expensive. Currently at Jagiellonian University a novel PET detector based on polymer scintilators is being developed. Using plastic scintillators one can reduce the cost of a scanner.

In 1980' the new method of scan called Time-of-Flight was introduced. First TOF-PET detectors were made of CsF and BaF_2 crystals, but those detectors had very low spatial resolution and sensitivity in comparison to BGO at that time. Availability of new scintillators (like LSO and LYSO) [5, 13], as well as improvements in the field of electronics and more choices of cost effective photomultipliers made studies on TOF-PET available. In 2005 Siemens TOF-PET scanner based on LSO achieved 1.2 ns timing resolution [6], a first commercial TOF-PET was constructed in 2006 by Philips and was based on LYSO crystals, this scanner achieved 650 ps (FWHM) resolution time, later in in 2007 Gemini TF scanner based on LYSO crystals achieved

even better result - 600 ps (FWHM) [11] and finally in 2008 Simens made a prototype scanner based on LSO crystals that achieved 550 ps (FWHM).

Spatial resolution along LOR is directly connected with time resolution of detector, which makes it the most important parameter that characterizes TOF-PET scanner. It gives us information about how well one can locate the point of annihilation using time difference between two detectors and it depends on few factors: type of photomultiplier and electronics used to analyse signals and most importantly on the type of scintillation material.

The main aim of this thesis is to determine spatial resolution of Strip PET as a function of the size of a patient's body, which in this case was imitated by phantoms filled with water and alcohol. In chapter 2 basics of physics behind PET are presented with description and comparison of currently produced PET scanners and Strip PET. In chapter 3, description of an experimental setup is presented. All measurements were conducted using a double detection module built out from BC420 plastic scintillator strips (with dimensions of 5 x 19 x 300 mm^3) read out at two ends by Hamamatsu R4998 photomultipliers. The measurements were performed using beam of annihilation quanta from the ^{22}Na isotope and the Serial Data Analyzer (Lecroy SDA6000A) which enabled sampling of signals with 100 ps intervals.

Description of measurement of speed of light along the scintillator strip and a beam profile are presented in chapters 4 and 5. Determination of these parameters is crucial for calculation of scanner resolution. In chapter 7, it is explained why certain phantoms were used in case of this study. Finally, in chapters 8 and 9 one can find the description of a method for determining time and spatial resolution of double module of a Strip PET scanner prototype. Calculations of both Time-of-Flight along the Line-of-Response and spatial resolution are presented.

2 PET detectors

PET scanners used nowadays in hospitals are constructed of many inorganic scintillators as a detectors of gamma quanta produced in annihilation process of electron and positron. These, in most cases two gamma quanta, are flying in opposite directions along the line (referred to as a Line-of-Response: LOR), with exactly defined energy equal to 511 keV. All detectors are formed in a ring around patient's body (Fig. 2.1). Two gamma quanta are considered to be a pair from annihilation if they hit opposite detectors within 5-10 ns [8]. Fluorine ^{18}F is the most common β^+ emitter used in hospitals due to its half life time, long enough to perform a scan and short enough not to have negative influence on a patient. This radionuclide is combined with a chemical substance and it is called radiopharmaceutical. This substance is responsible for delivering a nuclide to part of a body which one wants to examine.

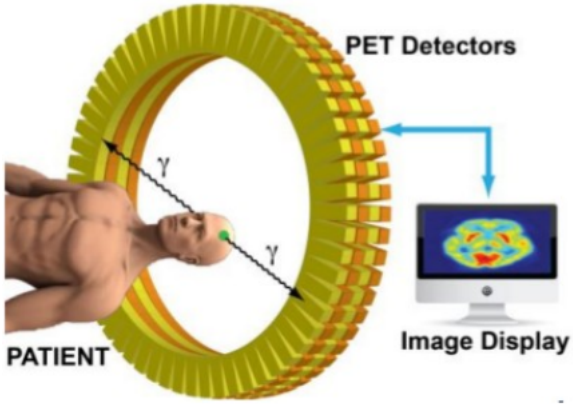

Figure 2.1: Schematic view of PET scanners used in hospitals. Figure adapted from [10].

When gamma quanta from annihilation hits a scintillator, it can transfer its energy, partially or entirely to an electron. This electron induces flashes of light in the process of ionization and excitation of atoms or molecules. Light flashes are then converted into electric signals by photomultiplier tubes

connected to scintillators.

Reconstruction of lines of response is essential to reconstruct tomographic image, which reflects the distribution of the density of the radiopharmaceutic in the body of the patient. PET is used to observe physiological processes that occur in body. Standard radiation dose given to patient during examination amounts to about 7 mSv, which is similar to other diagnostics techniques [13]. Therefore, PET has no negative influence on a patient, due to hormesis mechanism it can even strengthen the immune system [11, 12].

2.1 Depth of Interaction

Positrons in the body created from β^+ decay of radionuclide are decelerating after being scattered during collision with electrons (their kinetic energy decreases to the value close to zero) then annihilation process occur on the average of few millimetres far from nucleus from which it was emitted. Another factor limiting accuracy of the detector is unknown depth at which gamma quanta reacts in scintillator.

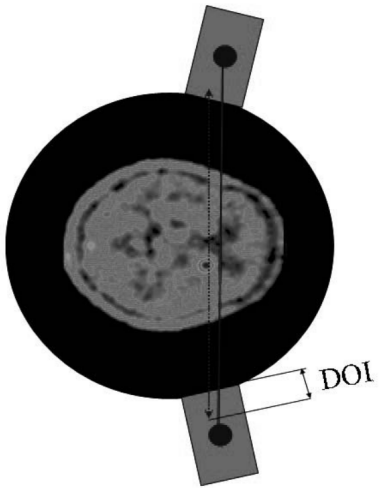

Figure 2.2: Schematic view of the reconstruction of the LOR with unknown depth of interaction. Figure adapted from [10].

Most inorganic scintillators are made in size of about 5 x 5 cm and 2.5 cm thickness. Additionally, they are cut into smaller units 0.5 x 0.5 cm [14]. Hit position reconstruction in crystal detector is based on the assumption that the position where gamma quantum was absorbed is in the middle of the unit. In Fig. 2.2 inaccuracy of this assumption is shown. Solid line shows LOR reconstructed, when one assumes that signal is created in the middle of the unit and dashed line presents the actual path of flight.

To improve an image reconstruction TOF method can be used, but in order to do it one needs a detector with good time resolution. This is the main reason why polymer scintillators were used in the case of this study.

2.2 Time-of-Flight

As it was mentioned before, by measuring the time difference between the arrival of the gamma quanta to the detectors, one can determine the point of annihilation along the Line-of-Response.

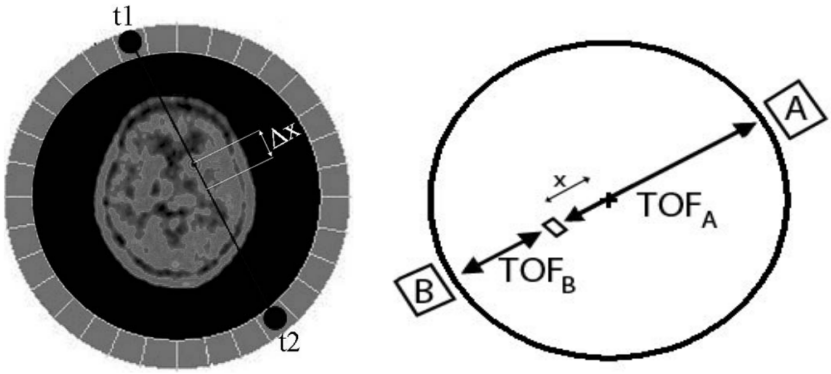

Figure 2.3: Schematic view of TOF-PET idea. Left figure is adapted from [10], right [21].

Reconstruction accuracy of the point where annihilation occurred relatively to the center of the LOR is limited by the finite resolution of time measurement (Fig. 2.3). As a result one can only determine the range in

which annihilation took place. Therefore, the better time resolution is, the more exact spatial resolution along Line-of-Response can be achieved. Time resolution of current PET scanners based on crystals amounts to about 550 ps (FWHM) [8,15], and it can be improved to about 265 ps when using a plastic scintillators [7].

Time-of-Flight can be determined from:

$$TOF_A = \frac{x}{c} + \frac{L/2}{c} \tag{2.1}$$

$$TOF_B = \frac{L/2}{c} - \frac{x}{c} \tag{2.2}$$

where: L denotes distance between detectors A and B, c - speed of light and x stands for the distance between point of annihilation and the center of LOR.

Difference between TOF for two detectors is:

$$TOF = TOF_A - TOF_B = \frac{2x}{c} \tag{2.3}$$

Uncertainty of the determination of the point of annihilation along LOR can be determined using following equation [2]:

$$\sigma\left(x\right) = \frac{\Delta t * c}{2} \tag{2.4}$$

where: $\sigma(x)$ - is localisation error, and Δt denotes error of determining time difference (TOF) between detectors A and B.

In Tab. 2.1 value of time resolution and its corresponding spatial resolution calculated with Eq. 2.4 is shown. TOF-PET detectors with inorganic scintillators have resolution of about 500 - 600 ps (FWHM) and the TOF resolution obtained for a single strip J-PET prototype is equal to about 265 ps [7].

Table 2.1: TOF resolution between two detectors and corresponding spatial resolution along the LOR line.

$\sigma(TOF)$ **[ps]**	$\sigma\,(x)$ **[mm]**
30	4.5
50	7.5
100	15
200	30
300	45
500	75
600	80

2.3 Strip PET detector constructed of polymer scintillators

Currently at Jagiellonian University a novel TOF-PET detector constructed of polymer scintillators is being developed. Schematic view of this device is shown in Fig. 2.4. Nowadays all scanners used in hospitals are based on crystal detectors, which have high density, detection efficiency and probability for photoelectric effect. For plastic scintillators these properties have very low value and therefore they were not used previously. Nevertheless, low density and efficiency can be compensated by improved time resolution and by placing several layers of strips around patient's body.

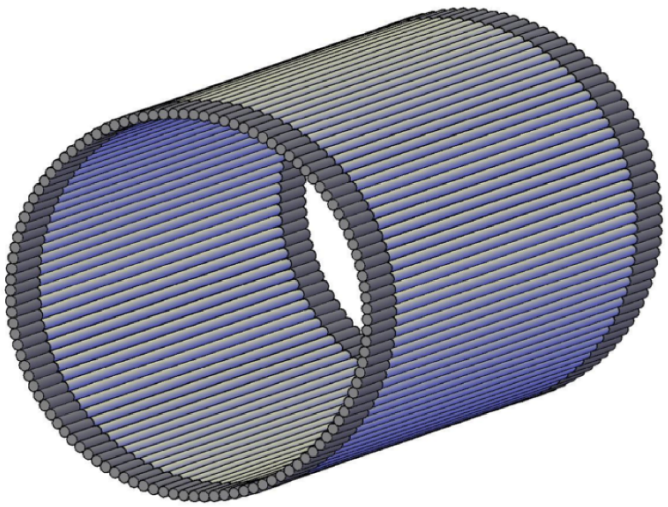

Figure 2.4: Strip PET detector. Patient would lie horizontally inside the barrel, along scintillator strips. Courtesy of T. Bednarski.

One of the biggest advantages of this device is not only the possibility of obtaining a better time resolution but, above all low production costs compared to currently used scanners. Mostly because the production of plastic scintillators is much cheaper, and it is easier to get different shapes and even very long strips, around 1 m. For example 1 cm^3 of crystal scintillator costs around 30 - 80 euro, while for polymer it's around 1 euro [16, 17, 20]. Lower costs of production and improved resolution will certainty make PET scanners more accessible for hospitals, especially in Poland.

Organic scintillarors are composed mainly of carbon and hydrogen [10]. Small atomic number is the reason for the negligible probability for photoelectric effect in polymer scintillators, which current scanners use for detection of gamma quanta. For crystals, energy window applied is in the range from 350 keV to 650 keV [18] and it corresponds to angular range of scattering from 0 to around 60 degrees. In polymer scintillators, Compton scattering is the main source of interaction. To get the same angular range of scattering one has to use an energy threshold of around 200 keV [9].

Linear absorption coefficient of gamma quanta with energy 511 keV for polymer is 0.098 cm^{-1}, it is eight times smaller than LSO (0.821 cm^{-1}) [8]. As a result, probability that two gamma quanta react in 2.5 cm thick layer is 16 times smaller for plastic scintillator than LSO one [9]. In spite of this, small efficiency can be compensated by the large acceptance and by placing multiple layers of strips in barrel.

Another advantage of Strip PET will be the possibility of imaging whole patient body in one scan. Additionally, large acceptance capability and good TOF resolution has increased the possibility of using a 3D mode of image reconstruction.

3 Experimental setup

If one wants to have the best possible time and spatial resolution of the Strip PET scanner, one needs to properly calibrate the setup. What is important is to test which kind of photomultipler, scintillator alignment and strips covering allows us to get the best time- and spatial resolution. In order to achieve this, tests with two different kind of photomultipliers, different scintillators alignment and foil covering strips were conducted. All measurements were done with double module of a Strip PET prototype constructed of polymer scintillators.

3.1 Velocity measurement

Setup shown in Fig. 3.1 was used for most measurements conducted with double model of Strip PET, inter alia to measure speed of light along scintillator strip. Setup for beam profile and phantom measurement was different, these differences are described in chapters 3.2 and 3.3

BC420 scintillators (Tab. A.1) made of polyvinyltoluene with dimensions of 5 x 19 x 300 mm^3 were connected with optical gel EJ550 to R4998 photomultipliers (Tab. B.1), made by Hammamatsu. Both strips were in horizontal alignment and wrapped in vikuiti foil. Photomultopliers were connected to CAEN SY4527 high voltage power supply. Signal from each photomultiplier was transferred via SMA cables to the corresponding channels of digital oscilloscope (LeCroy SDA 6000A) and probed within 100 ps intervals.

Applied voltage was set in a way that the gain on all photomultipliers was the same. ^{22}Na source were placed inside of lead collimator with a 1.5 mm slit. Sodium source had activity of around 18.5 MBq. Each lead slice of collimator has dimensions of 5 x 10 x 20 cm. Mechanical step motor was used to move

collimator to the exact position along whole length of scintillator with an accuracy better than 0.1 mm.

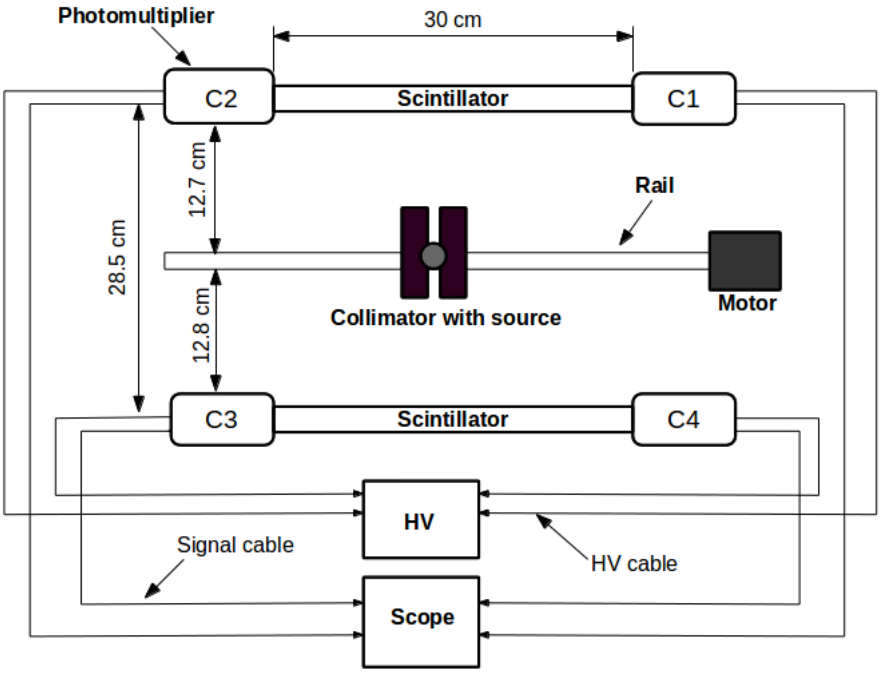

Figure 3.1: Setup used for tests measurements and determination of velocity. C1, C2, C3, C4 stands for SDA channel number to which corresponding photomultiplier was connected. Signals from photomultiplier were sampled in time domain by scope LeCroy SDA6000A. Radioactive source was placed inside of lead collimator which could be moved by motor along scintillators. Abbreviation HV denotes high voltage power supply CAEN SY4527.

3.2 Beam profile measurement

For beam profile measurement photomultipliers were changed to R9800 (Tab. B.2). To measure the profile of annihilation gamma quanta, lead "shadow" was placed between the collimator and a scintillator, as it is shown in Fig. 3.2. Shadow consisted of two or one lead bricks, depending on the method of measurement. The thickness of the brick was equal to 5 cm.

Slit between lead bricks and collimator were exactly parallel to each other and centers of both slits were on one line. When only one brick was used,

the second one was taken out without any other changes in the setup.

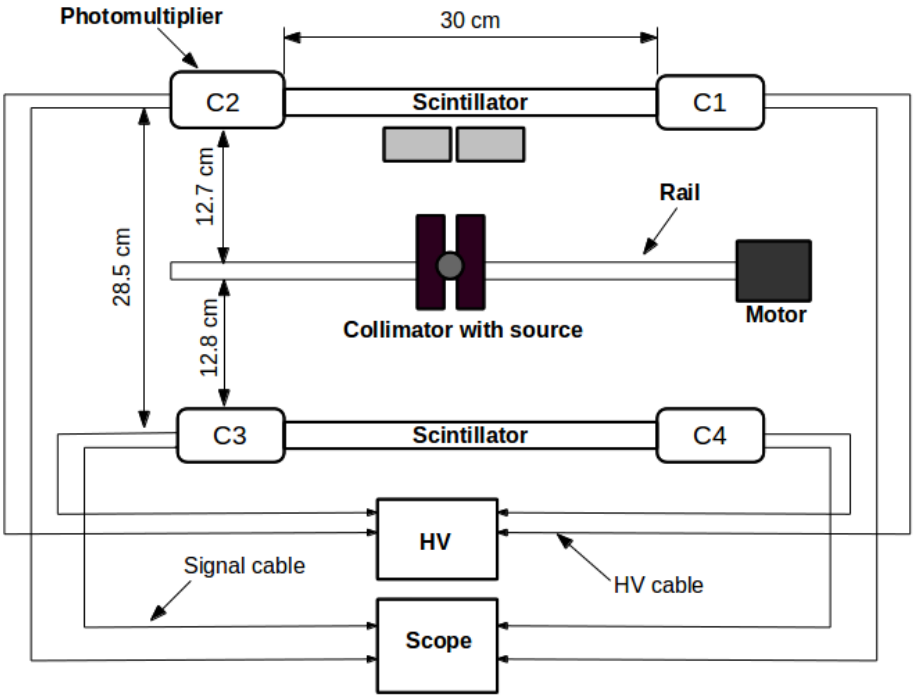

Figure 3.2: Setup used for beam profile measurement. As one can see on setup shown in Fig. 3.1 lead bricks with thickness of 5 cm were added as a "shadow" between the collimator and one of the scintillators.

3.3 Phantom measurement

Setup for the phantom measurements is shown in Fig. 3.3. As one can see, there is no collimator, and radioactive source was sealed in a plastic round radioactive source with diagonal of 2 cm. This box was then placed inside the phantom, which was then filled with water or alcohol. Phantom was placed at the central position with respect to scintillators.

In this part of measurements four phantoms with different sizes were used. Their dimensions and description are given in chapter 6.

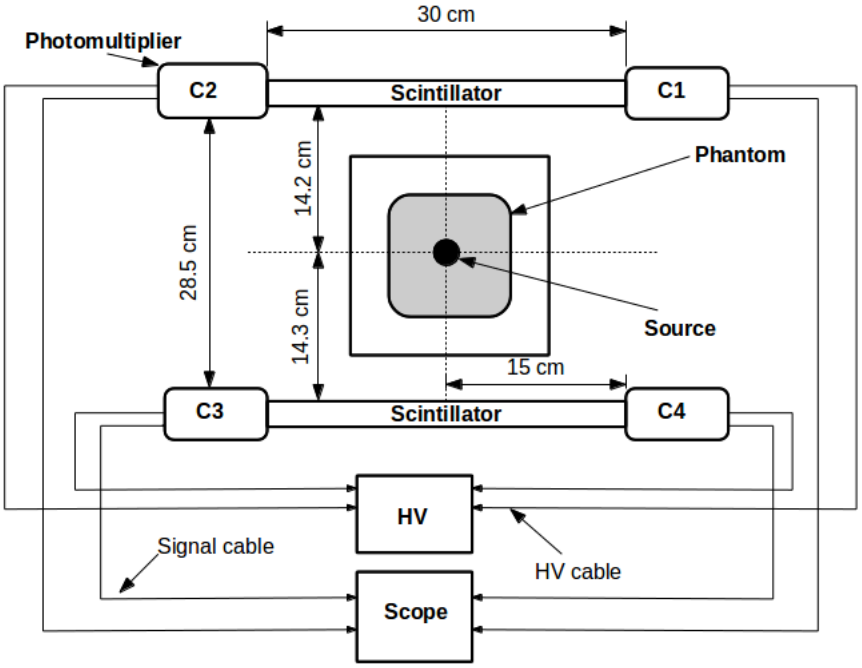

Figure 3.3: Setup for phantom measurements. Radioactive source is sealed in a round pan, which is placed inside of the phantom. Source is placed exactly at the central position relative to the scintillators.

All settings, such as voltage applied, threshold and trigger for each measurement are described in Appendix C. Additionally, some properties of scintillators and photomultipliers are also presented in Appendixes A and B, respectively.

4 Determination of a beam profile

Spatial distribution of the beam of annihilation quanta used in the measurements influences the results obtained for parameters such as time- or spatial resolution. These parameters become very important when it comes to acquiring a high quality image of a patient's body. Therefore beam profile was determined using two different methods.

In this thesis two methods to determine beam profile are described. In first method only one lead brick was used as a "shadow", shown in Fig. 3.2. Second brick was removed for the time of measurement. In second method both bricks were used at the same time. Measurements were done by moving collimator along the rail. Number of events with coincident signals in both strips were measured for 15 minutes per each position.

4.1 Method I

In order to determine the beam profile h(x) the detector is irradiated by the tested beam which can be shifted with respect to the detector along the x-axis. The measured number of events as a function of x can be expressed as a convolution of the beam profile and the detector acceptance function:

$$M(x) = h(x) * g(x) = \int_{-\infty}^{+\infty} h(x - x')g(x')dx' \tag{4.1}$$

In the case of large single shadow block absorbing gamma quanta in the range from x_0 to $+\infty$. The function of the acceptance of a detector can be approximated by:

$$g(x) = \begin{cases} 0 & if \quad x \in [x_0, +\infty] \\ 1 & if \ x \notin [x_0, -\infty] \end{cases} \tag{4.2}$$

This implies that all events which are within this section are being accepted, other signals are being rejected. Applying equations 4.1 and 4.2 one obtains:

$$M(x) = h(x) * g(x) = \int_{-\infty}^{x_0} h(x - x')dx' \tag{4.3}$$

By derivation of equation (4.3) one can extract the relation for the beam profile:

$$\frac{d}{dx}M(x) = h(x - x_0) \tag{4.4}$$

In this part of beam profile measurements only one brick was used. It was placed near C1 and C2 PM side (as shown in Fig. 3.2). Its position relative to the strip has not changed, simply one of the bars was removed. In Fig. 4.1 (left) an exemplary distribution M(x) obtained in the measurement is shown. This distribution corresponds to the function M(x) defined in equation 4.3.

To extract shape of beam profile numerical derivative of M(x) needs to be calculated using Eq. 4.5:

$$h(x) = \frac{dM}{dx} = \frac{N_2 - N_1}{x_2 - x_1} \tag{4.5}$$

where: N_1, N_2 denote number of counts in consecutive measurements, x_1, x_2 - consecutive positions. The uncertainty of h(x) was calculated as:

$$\sigma = \frac{\sqrt{N_2 + N_1}}{x_2 - x_1} \tag{4.6}$$

In Fig. 4.1 M(x) distribution (left) and beam profile h(x) (right) from measurement with step of 0.1 mm are shown. To each h(x) Gauss function was fitted in order to extract FWHM and sigma values that corresponds to the beam profile width.

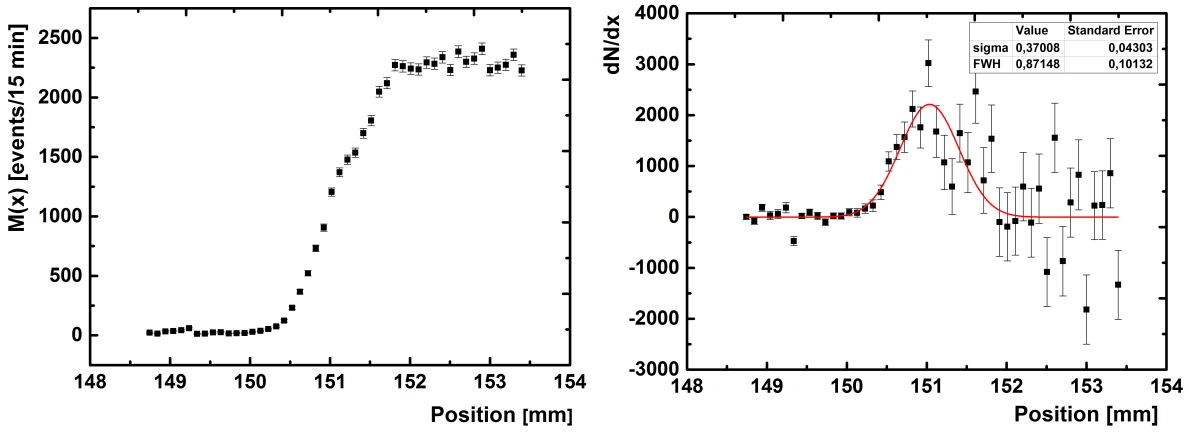

Figure 4.1: (left)Number of coincidences as a function of the relative position between the collimator and left bar of the shadow positioned close to the scintillator strip read out by photomultipliers C1 and C2. The slit of the collimator was equal to 1.3 mm. Scintillators were aligned horizontally. The measurement started at position 148.4 mm, was conducted with step of 0.1 mm and finished at 153.4 mm.(right) Derived beam profile with fitted Gauss function.

Additionally, using data from spectra shown in Fig. 4.1, new spectra were created, where each point was the average value of the two values, respectively, the x and y axes of neighbouring points. Then, to this points Gauss function was fitted in order to extract beam profile. Results are shown in Fig. 4.2.

As one can see in Fig. 4.2 beam profile is smoother than before. The reason for big errors and spread of points in Fig. 4.1(right) was smaller statistics per measurement point. Calculating the average of two points allows to decrease the statistical errors. It is important to note that before and after averaging the determined beam profile width is the same within uncertainties.

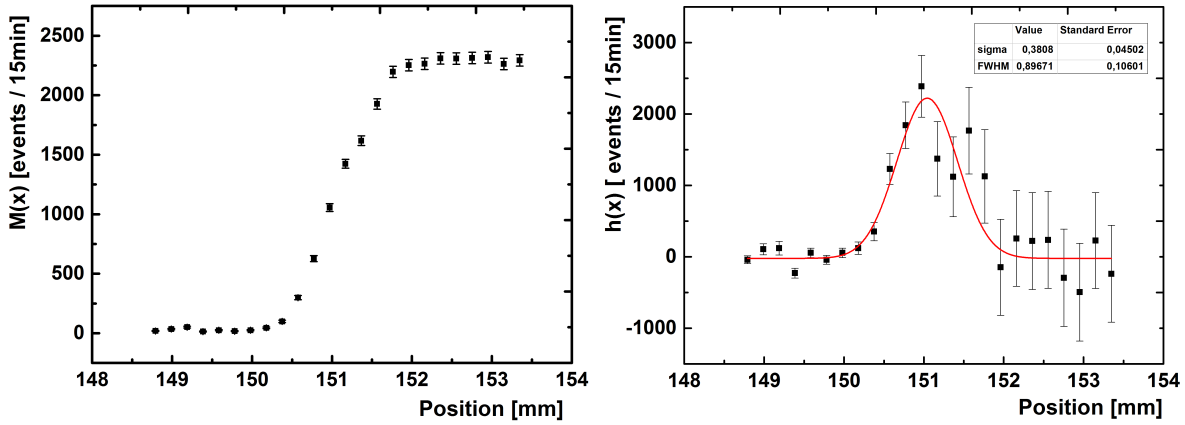

Figure 4.2: (left)Number of coincidences as a function of the relative position between the collimator and right bar of the shadow positioned close to the scintillator strip read out by photomultipliers C1 and C2. The slit of the collimator was equal to 1.3 mm. Scintillators were aligned horizontally. Data points were calculated as the average value of two neighbouring points from Fig. 4.1.(right) Derived beam profile with fitted Gauss function.

4.2 Method II

In this part of experiment additional lead brick was placed, as it is shown in Fig. 3.2. So now we have a slit in the "shadow" parallel to the collimator slit, as a result we receive beam profile directly from the measurement, without any additional calculation.

In Fig 4.3 method of measurement is shown in a pictorial way. Measurement was done by moving collimator by a few centimeters around from the center with a step of 0.3 mm.

Below in Fig. 4.4 results from all measurement with two lead bars as a shadow are shown. For each Gauss function was fitted in order to extract FWHM and sigma values that corresponds to the beam profile width.

The reason for the asymmetric shape of the beam profile most probably was that the bar's surfaces were not perfectly smooth.

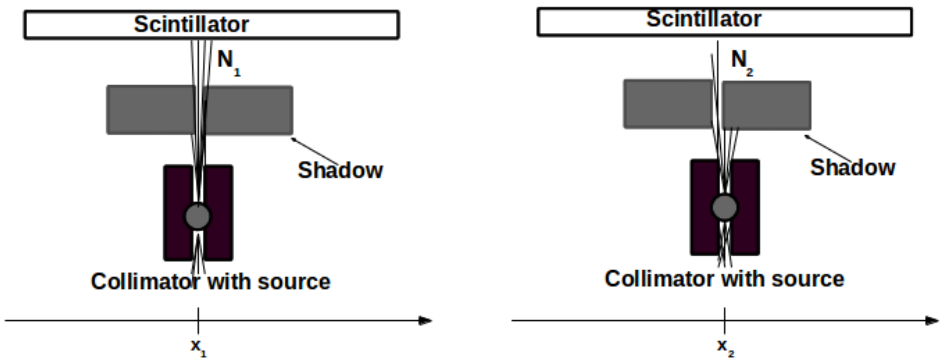

Figure 4.3: Scheme illustrating method of the measurement.N_1 and N_2 denote number of events measured in a given time interval at positions x_1 and x_2, respectively.

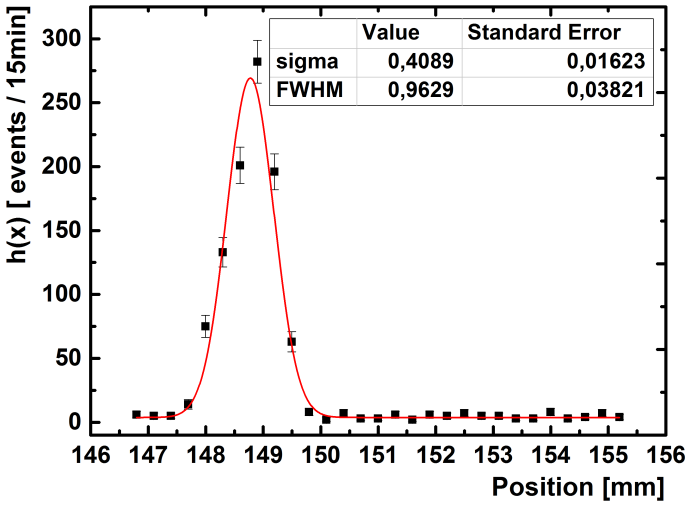

Figure 4.4: Number of coincidences as a function of the relative position between the collimator and the shadow. The shadow with a slit of 0.3 mm was positioned close to the scintillator strip read out by photomultipliers C1 and C2. The slit of the collimator was equal to 1.3 mm. Scintillators were aligned horizontally. The measurement started at position 146.8 mm, was conducted with step of 0.3 mm and finished at 155.2 mm.

In Table 4.1 beam profile width values for both measurements methods are presented.

Table 4.1: Values of FWHM as a beam profile width from Gaussian fit.

Measurement	**FWHM [mm]**
Method I	0.87(10)
Method I - average of two points	0.90(11)
Method II	0.96(04)

As one can see from Table 4.1 the width of the beam profile is basically the same within measurement uncertainty range for both methods and it is equal to $\sim$1 mm. Method II can be used as a model for the profile, but it cuts out all gamma quanta, which don't travel perpendicular to the scinillator.

It can be noted that the above described methods allow to define the profile of a collimated beam used for determining the parameters, such as time- and spatial resolution of the Positron Emission Tomography.

5 Speed of light signals along a scintillator strip

In order to determine the Time-of-Flight resolution of PET scanner one needs to know the speed of light signals along a scintillator strip. To this end, a scan of a whole strip was done, and then straight line was fitted to the time difference Δt as a function of the irradiation position x. From fit one can extract the velocity v. Time difference is equal to:

$$\Delta t = t_R - t_L \tag{5.1}$$

where: t_R - time from right photomultiplier and t_L left photomultiplier.

Scan of the scintillator was done using setup shown in Fig. 3.1. Measurement was performed for 20 positions of irradiation. Time difference at 80 mV threshold was derived for both scintillators as a function of the irradiation position. The result is shown in Figs. 5.1 and 5.2. Velocity was calculated as:

$$v = \frac{2}{b} \tag{5.2}$$

where b denotes the slope parameter from fitted line.

The walk effect was not taken into account in case of this thesis. In future study both walk effect and the variation of the average amplitude of signals as a function of the distance between the interaction point and photomultipliers will be included.

Results are shown in Fig. 5.1 and 5.2 and calculated velocity for both strips is presented in Table 5.1. Straight line was fitted to all points except to the first and the last one to avoid influence of border effects.

The resulting speed of light given in Table 5.1 determined for a single

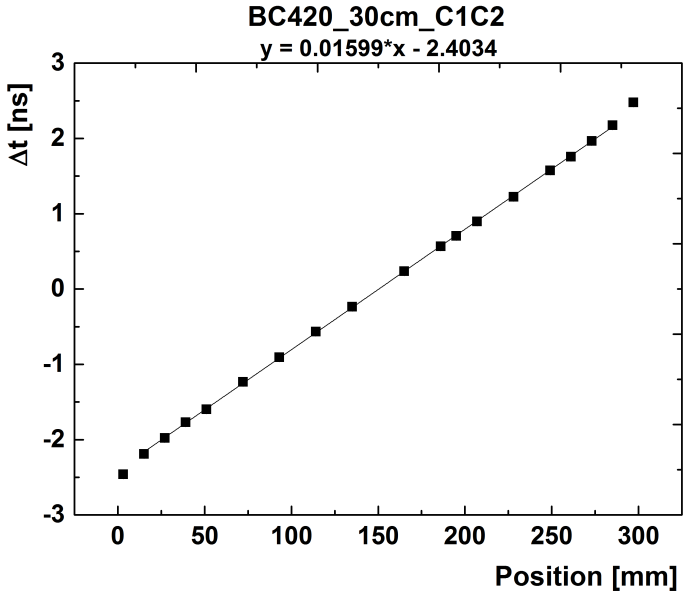

Figure 5.1: Mean time difference as a function of the irradiation position x with fitted straight line for first scintillator.

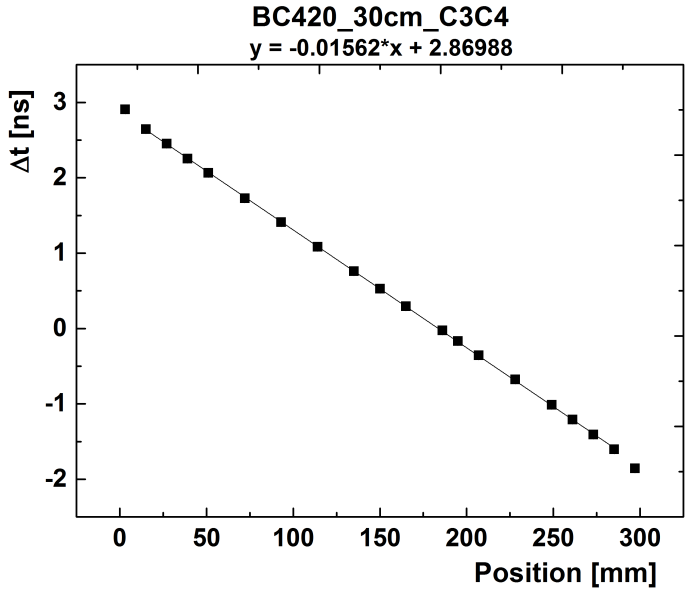

Figure 5.2: Mean time difference as a function of the irradiation position x with fitted straight line for second scintillator.

module of the Strip PET prototype is compared with velocities for both organic and inorganic scintillators (Tab. 5.2).

The speed of light signals depends not only on the material used but also

Table 5.1: Speed of light signals along the scintillator for both strips.

Scintillator	**Velocity [cm/ns]**
C1C2	12.51(05)
C3C4	12.80(05)

Table 5.2: Speed of light signals along the strip for different kinds of scintillators.

Name	**Type**	**Dimensions [cm^3]**	**Velocity [cm/ns]**
BC420	Polymer	0.5 x 1.9 x 30	12.51
BGO	Crystal	4 x 19 x 300	16.05 [22]
BC404	Polymer	2 x 10 x 95	15.7 [23]
Plastic	Polymer	0.8 x 12 x 40	10 [24]

on the cross section of the strips. In general the lower is the velocity the better the spatial resolution.

6 Phantoms as a simulation of the patient's body

The aim of this thesis is to determine the impact of the patient's body size on a spatial resolution of a Strip PET. Since all studies for this thesis were done using double module of a PET prototype there was no possibility to do measurement on actual patient. As such, object that would simulate a body was needed. To do so, phantom was made from substances which have similar density as human tissues [26, 28].

To this end we have used plastic boxes filled with water or ethyl alcohol. The plastic material was 2 mm thick only, and its density is comparable with the density of the water. Phantoms were filled first with water that has similar density as a soft tissue and then with ethyl alcohol which density correspond to fat tissue. In case of this thesis four different sizes of phantoms were used.

All measurements were done without collimator. Sodium source, that was sealed in round plastic pan, was placed directly in the center of each phantom. Then phantom was filled with appropriate fluid to a hight of around 3.5 cm, so the pan was completely covered.

In Table 6.1 sizes of phantoms used for studies of PET resolution are presented. Also picture of a phantom placed in setup, which one can also see on scheme in Fig. 3.3, is shown in Fig. 6.1. All phantoms measurements were done in a way that source was placed exactly at a central position with respect to the scintillator.

Similar phantoms are used to calibrate different kind of tomographs in hospitals [29]. Water is the best substance which imitates human tissue, due to its density, in case of these kinds of experiments. Basically phantoms that are

Figure 6.1: Picture of a phantom used for measurement, inside one can see pan with the source.

Table 6.1: Sizes of phantoms used for measurements.

Phantom number	**Size [cm]**
I	8 x 8
II	10.5 x 10.5
III	12.5 x 12.5
IV	22.5 x 14.5

used allow doctors and technicians in hospitals to calibrate and check scanner by themselves, without any external assistance, which definitely lowers the costs of maintenance.

7 Studies of time resolution

Due to fast signals from plastic scintillators one can achieve high resolution for Time-of-Flight measurements. The higher the resolution is the better the time difference between two signals can be established. The time resolution depends on the amount of number of photo-electrons produced in the converter to the duration of the signal [1]. That quality is better for plastic scintillators, which have decay time less than 2 ns and large light output of 10 000 photons/MeV, while inorganic scintillators such as LSO have decay time 40 ns and light output of 32 000 photons/MeV. The fact that in polymer scintillators this parameters are better than in inorganic ones decreases the noise along the Line-of-Response and makes it possible to have good 3D image reconstruction for the detector with large Field-of-View [2].

Since 1980 companies tried to create PET detectors based on the Time-of-Flight method. Because of a very slow signals in inorganic scintillators is not very effective. After the discovery of LSO and LYSO crystal in 2006 first commercial TOF-PET scanner was constructed by PHILIPS, achieving a TOF resolution of 650 ps (FWHM) using LYSO scintillators. Two years later, in 2008 SIEMENS made a prototype based on LSO scintillators with resolution of about 550 ps (FWHM). That value corresponds to the spatial resolution along the Line-of-Response of about 8 cm [2, 8].

7.1 Time-of-Flight calculation

Firstly, one has to determine the distribution of time differences between arrival of signals from each side of a module (Fig. 7.1):

$$\Delta T_{C1C2} = t_{C1} - t_{C2} \tag{7.1}$$

$$\Delta T_{C3C4} = t_{C4} - t_{C3} \tag{7.2}$$

where: T_{CiCj} - time difference for single module, t_{Ci} - time when signal was register from Ci photomultiplier was registered.

Secondly, the time at which gamma quantum hits the module needs to be determined. It can be done by calculating the arithmetic mean of times measured on both sides of each module:

$$T_l = \frac{t_{C1} + t_{C2}}{2} \tag{7.3}$$

$$T_r = \frac{t_{C4} + t_{C3}}{2} \tag{7.4}$$

where: l - left strip, r - right strip, t_{Ci} - time when signal was register from Ci photomultiplier was registered.

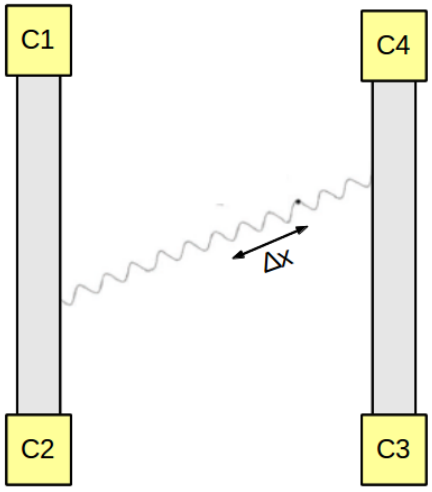

Figure 7.1: Scheme of two modules of the J-PET detector.

Registration of two gamma quanta in coincidence allows to determine the Line-of-Response, based on coordinates of reaction points reconstructed in both strips [10]. Time-of-Flight was determined using equation:

$$TOF = \frac{t_{C1} + t_{C2}}{2} - \frac{t_{C4} + t_{C3}}{2} \tag{7.5}$$

7.2 Method of determination of the Time-of-Flight resolution

In order to calculate TOF value for each phantom, several operations had to be done. Phantoms (Tab. 6.1) with radioactive source were measured using the setup shown in Fig. 4.3. Only those signals that appeared simultaneously on all four photomultipliers were measured, thus allowing for collection of signals coming from annihilation events.

After rejecting of noise, for further analysis only these signals were used which charge was larger than 30 pC. An exemplary charge spectra before and after cut for measurement with empty phantom without fluid is shown in Fig. 7.2.

For all events after the cut on the charge, time differences in a single module at threshold 80 mV were calculated using Eq. 7.1-2. In Fig. 7.3 one can see results for both strips from measurement with phantom without fluid.

As one can see the spectra has width of about 5 ns, what corresponds to the length of the scintillator (30 cm). Offset between both spectra has no implication for the further study and is related to the different length of cables. Because all these measurements were not done with collimated beam, to calculate TOF, one needs to divide this spectra into intervals to have data from each centimeter of the strip separately. Knowing the speed of light along scintillator strip, one can calculate that to travel the distance of 1 cm signal

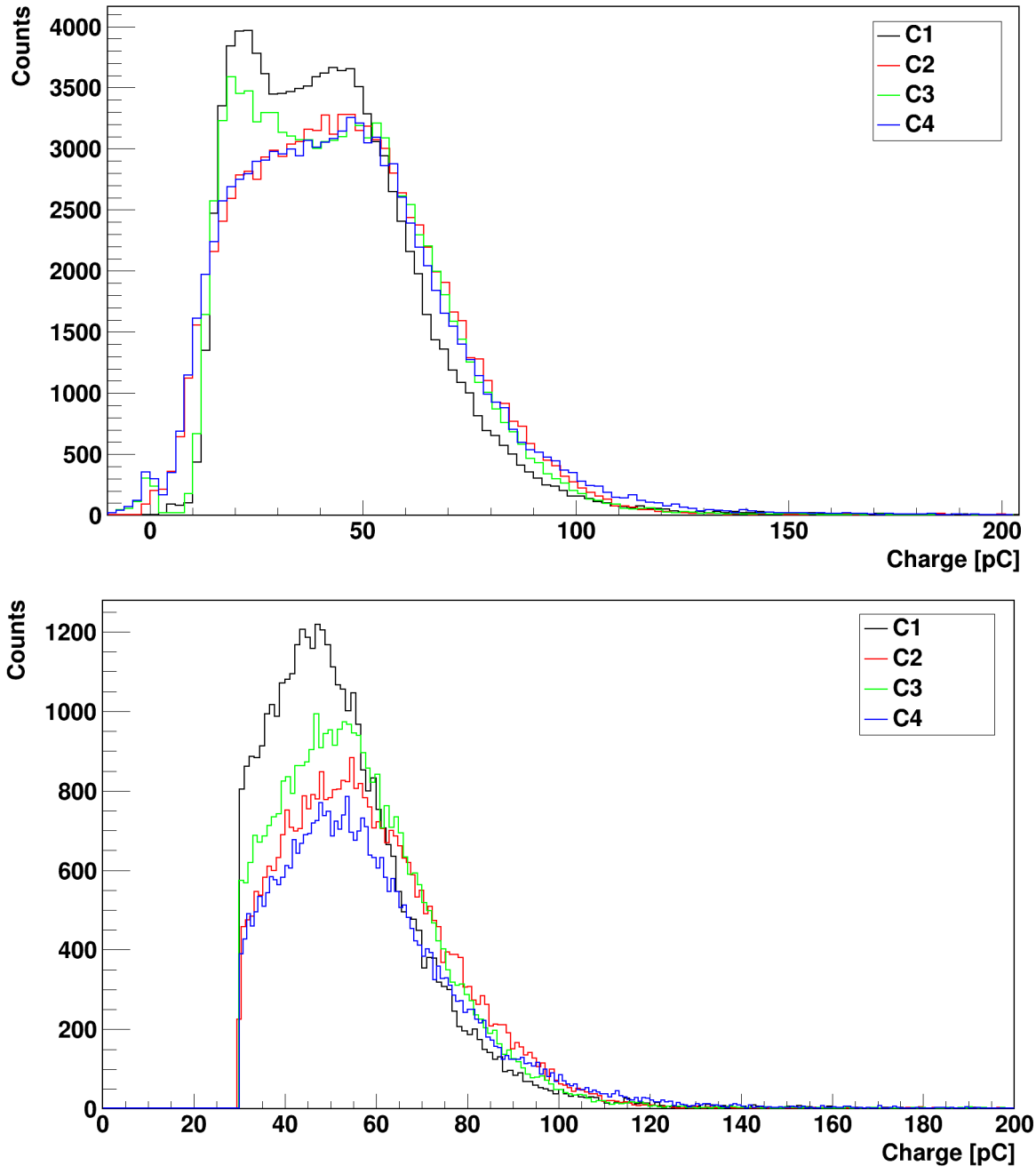

Figure 7.2: Charge spectra for measurement of phantom not filled with water or alcohol. (up) Spectra before cut on charge (bottom) after cut on 30 pC. C_i - stands for ith photomultiplier.

needs 0.16 ns (chapter 5). Taking mean of time difference distribution for each strip as a value corresponding to the center of the strip, whole spectra was divided into 0.16 ns intervals corresponding to 1 cm length.

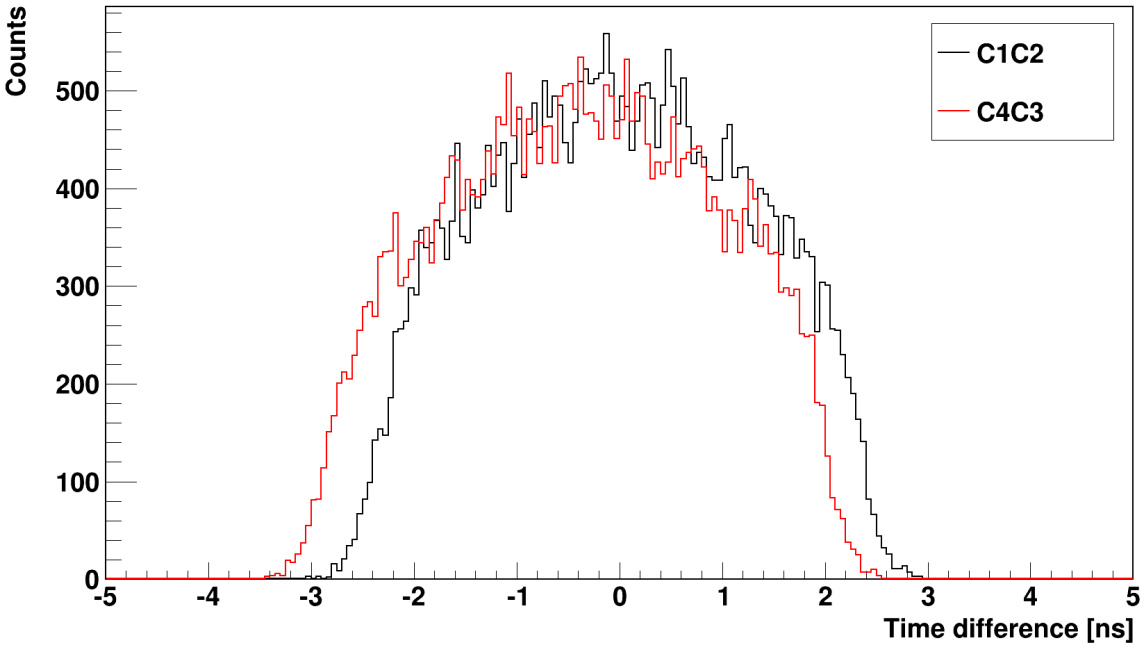

Figure 7.3: Distribution of time differences between arrival of signals to opposite ends of the strip.

Time differences for all ranges per strip for both scintillators from measurement without fluid are shown in Fig. 7.4. Offset for all measurements was around 0.4 ns.

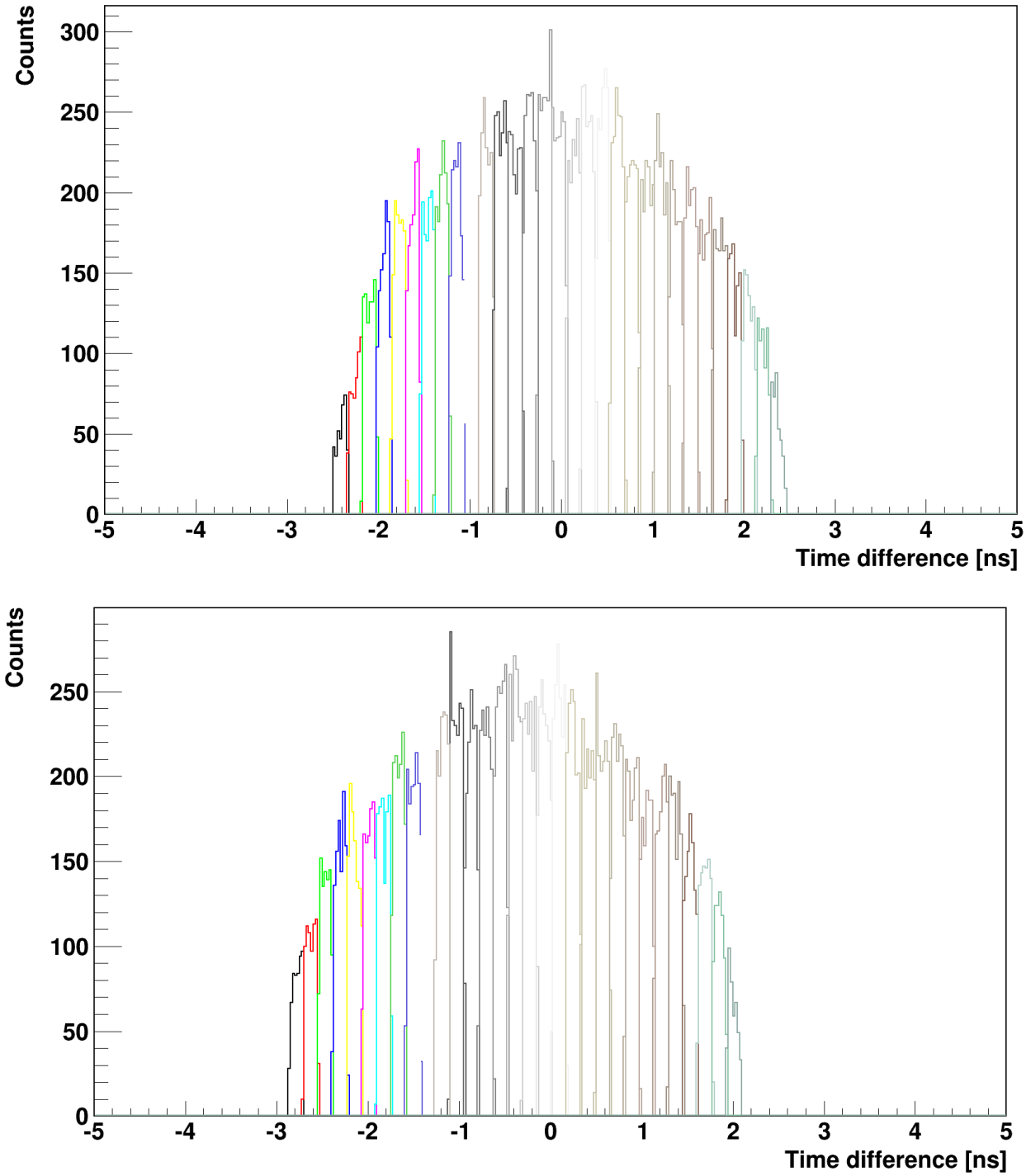

Figure 7.4: Distribution of time differences between arrival of signals to the opposite ends of the module. The spectra are divided into intervals corresponding to 1 cm range of the strip. On the upper spectrum results for the C1C2 strip, on the bottom for C3C4 strip are shown.

In Fig. 7.5 exemplary histograms of central interval from Fig. 7.4 are shown.

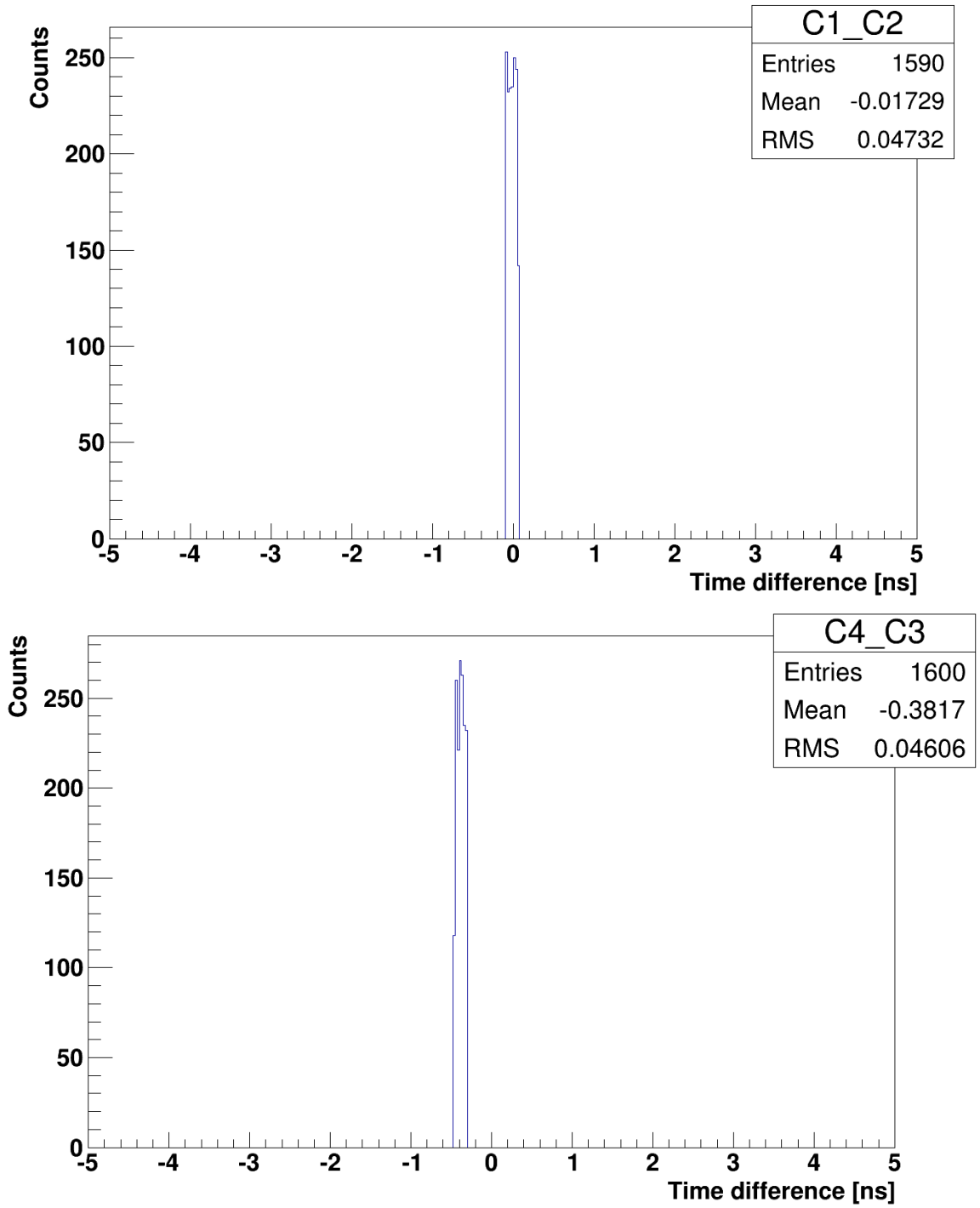

Figure 7.5: Distribution of time differences between arrival of signals to the opposite ends of the module for center interval for both strips. On the upper spectrum results for the C1C2 strip, on the bottom for C3C4 strip are shown.

In order to calculate TOF a timing of both strips has to be properly matched with each other. Looking at Fig. 7.1 one can imagine scintillators being divided into thirty 1 cm long intervals. As a first pair, intervals closest to C1 and C3 were taken, then next and so on. In this case the last pair of intervals correspond to the range of the scintillators closest to the to C2 and C4.

Within each pair of intervals Time-of-Flight was calculated using equation 8.5, gauss function was fitted to the histogram and sigma value of this fit was used as a measure of the TOF resolution. In Fig. 7.6 exemplary TOF histogram from measurement with empty phantom is shown.

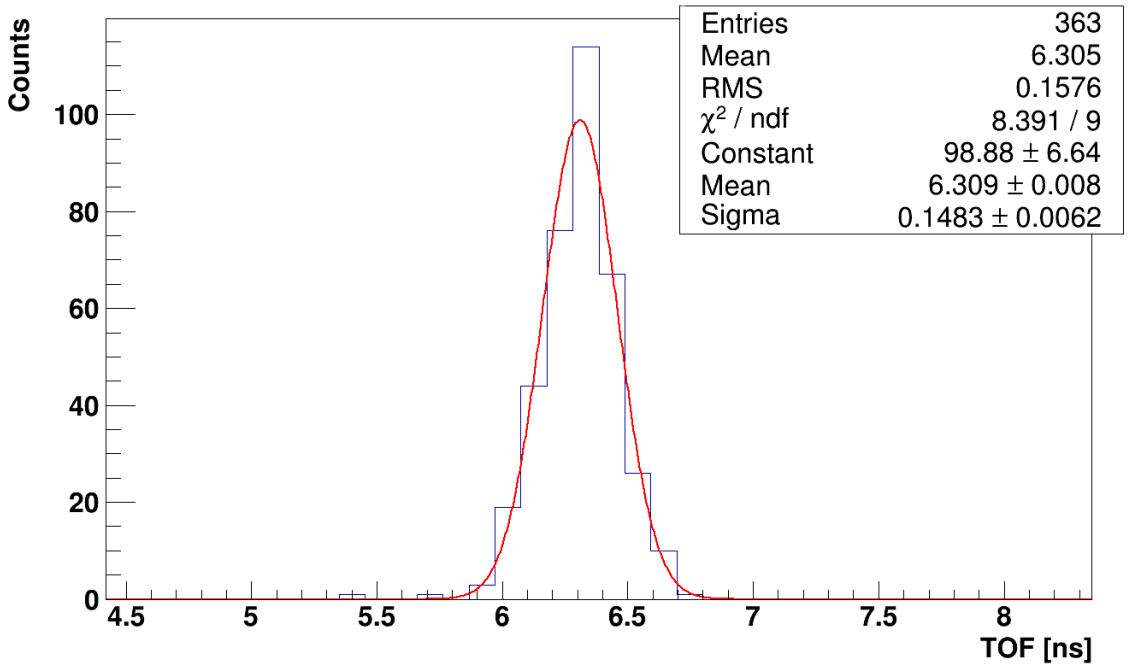

Figure 7.6: Time-of-Flight for central pair of intervals from measurement with empty phantom.

In the end, Time-of-Flight resolution as a function of pairs of intervals was drawn. Uncertainty of each point is taken from gauss fit. For some phantoms measurements first and last point were not taken into account, due to very low statistic in that range.

In Fig. 7.7 result for measurement with empty phantom is shown. Intervals pair number 1 corresponds to intervals closest to C1 and C3, while interval number 30 is closest to C2 and C4.

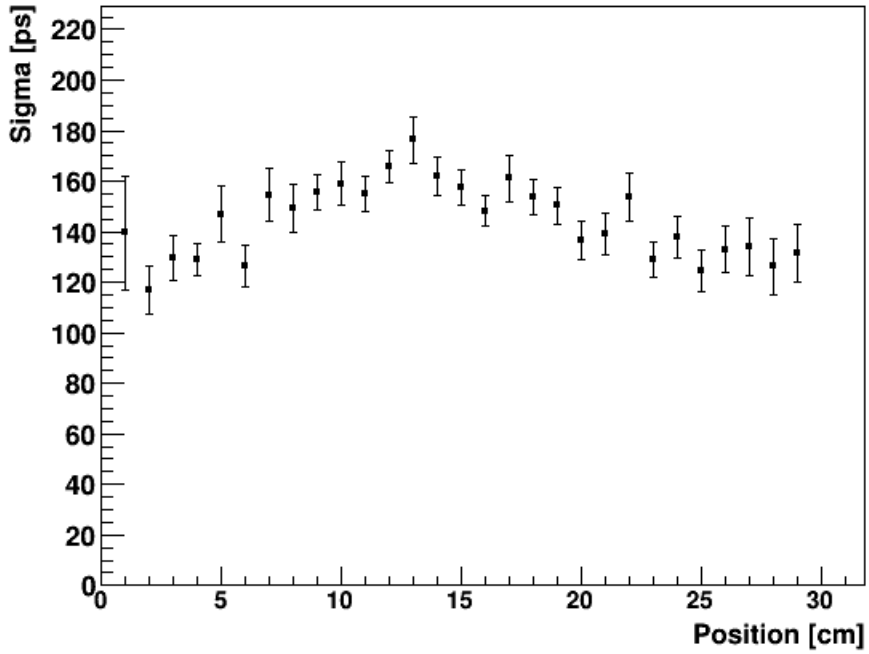

Figure 7.7: Time-of-Flight resolution as a function of position along the strip from both scintillators for measurement without fluids.

7.3 Results of Time-of-Flight resolution for different phantom sizes

Results of determination of the time difference between arrival of signals from the ends of a module for all phantom measurements are shown in Appendix E.

In order to determine Time-of-Flight resolution for each phantom filled with water and ethyl alcohol, arithmetic mean of sigma TOF value for each pair of intervals was calculated with standard deviation as an uncertainty. Resultant spectra with TOF resolution as a function of pairs of intervals for all phantoms are shown in Appendix G.

In Tab. 7.1 results of the determined Time-of-Flight resolution for different phantom sizes are presented. Phantoms were filled with water and ethyl alcohol, and measurement with empty phantom without water was used as a reference. Numbers I-IV correspond to sizes of phantoms, presented in Tab. 6.1.

Table 7.1: Time-of-Flight resolution for different phantom sizes.

Phantom	σ**(TOF) [ps]**
Water I	147 ± 14
Water II	145 ± 16
Water III	145 ± 17
Water IV	148 ± 14
Alcohol I	147 ± 15
Alcohol II	147 ± 18
Alcohol III	145 ± 17
Alcohol IV	145 ± 16
Empty	144 ± 15

For all phantoms, both those filled with water and with alcohol Time-of-Flight resolution is the same within the uncertainty range and equal to around 146 ps. This results is two times better than TOF resolution of commercial scanners used in hospitals nowadays.

8 Studies of spatial resolution as a function of the phantom size

Because of finite resolution of time measurement, one can only determine a range along LOR in which annihilation took place. Nowadays TOF-PET scanners with inorganic scintillators give a spatial resolution along the LOR of about 550 ps (FWHM).

Much better time and as a consequence spatial resolution along LOR is achievable with plastic scintillators, which were not used before due to their low efficiency for detection of gamma quanta, but efficiency can be improved by increasing thickness of scintillator.

Next important factor influencing the resolution of PET images can be size of a patient's body. However, in scanners used nowadays in hospitals it plays a big part in adjusting method of reconstruction, so that size of a body did not influence the resolution [31]. But mostly these scanners do not use Time-of-Flight method. Experiments in which standard and TOF-PET were compared, showed that using TOF method one can achieve better resolution [26]. Spatial resolution for different sizes of phantoms proves to be more or less the same [27, 28].

8.1 Method for determination of spatial resolution along the LOR

Position Δx (Fig. 7.1), is the distance between the point where annihilation took place and the central point of two strips, along the Line-of-Response. It is determined from time difference between two modules [9, 27].

$$\Delta x = \left(\frac{t_{C1} + t_{C2}}{2} - \frac{t_{C4} + t_{C3}}{2} \right) * \frac{c}{2} = \frac{TOF * c}{2} \tag{8.1}$$

Therefore spatial resolution along the Line-of-Response is equal to:

$$\sigma(\Delta x) = \frac{\sigma(TOF) * c}{2} \tag{8.2}$$

where: $\sigma(TOF)$ denotes the resolution of TOF determination and c denotes speed of light in vacuum.

8.2 Results of spatial resolution for different phantom's sizes

Spatial resolution for each phantom was calculated as an arithmetic mean from $\sigma(\Delta x)$ for all intervals. Uncertainty of this determination was calculated as a standard deviation.

Results for all phantoms are presented in Tab. 8.1. Numbers I-IV correspond to sizes of phantoms, presented in Tab. 6.1.

Table 8.1: Spatial resolution along Line-of-Response for different phantom sizes.

Phantom	$\sigma(\Delta x)$ **[mm]**
Water I	22.0 ± 2.2
Water II	21.7 ± 2.3
Water III	21.8 ± 2.5
Water IV	22.2 ± 2.1
Alcohol I	22.1 ± 2.3
Alcohol II	22.0 ± 2.7
Alcohol III	21.7 ± 2.5
Alcohol IV	21.8 ± 2.4
Empty	21.6 ± 2.2

For all phantoms spatial resolution along Line-of-Response is the same within the uncertainty range and it is equal to around 22 mm. This result is better by the factor of two in comparison to commercial TOF-PET detectors based on inorganic scintillators [27]. Taking into account that all measurements were done without walk correction, given result can be improved. Def-

initely after applying this correction and collecting data with much higher statistic even better spatial resolution of Strip PET will be achievable.

9 Summary and conclusions

The main aim of this thesis was to determine the spatial and Time-of-Flight resolution of the double module of Positron Emission Tomography prototype constructed of polymer scintillators, as a function of the patient's size. For the purpose of the investigation described in this thesis a radiopharmaceutical was simulated by a ^{22}Na radioactive source and the human body was imitated by water or ethyl alcohol filled in the plastic containers.

Gamma quanta from the annihilation of positron in the center of the phantom were registered by the double strip prototype of the J-PET detector. Each scintillator was read out by two photomultipliers, thus giving four signals in case if both annihilation quanta were registered.

Four different sizes of phantoms were measured, and for each one about 10^4 events were collected. In the analysis for each event a time differences between registration of light signals by photomultipliers were calculated and the TOF distribution was established for each 1 cm range of the tomograph.

The determined TOF resolution amounts to about 146 ps (sigma) and is fairly independent of the position of interaction. This results implies that the spatial resolution of the reconstruction of the annihilation point along the Line-of-Response is equal to about 22 mm (sigma). Obtained results are about two times better with respect to the current commercial PET scanners.

Appendix A

Properties of scintillator materials - comparison of crystal and polymer detectors

Table A1: Properties of scintillators material [20, 32–34].

Name	**Type** g/cm^3	**Density [ns]**	**Decay Time**	**Photons/MeV [cm]**	**Mean free path**
BGO	Crystal	7.13	300	6k	1.04
GSO	Crystal	6.71	50	10k	1.49
LSO	Crystal	7.40	40	29k	1.15
BC404	Polymer	1.032	1.8	10k	-
BC420	Polymer	1.032	1.5	10k	10.2

Appendix B

Properties of photomultipliers

Table B1: Properties of R4998 photomultipliers made by Hammamatsu [35].

Type	**Head - on type**
Spectral response [nm]	300 - 650
Dynode Structure	Linear-focused
Dynode Stages	10
Gain Typ.	$5.7*10^6$
Rise Time [ns]	0.7
Transit Time Typ. [ns]	10
Transit Time Spread [ns]	0.16
Photocathode Material	Bialkali

Table B2: Properties of R9800 photomultipliers made by Hammamatsu [36].

Type	**Head - on type**
Spectral response [nm]	300 - 650
Dynode Structure	Linear-focused
Dynode Stages	8
Gain Typ.	$1.0*10^6$
Rise Time [ns]	1.0
Transit Time Typ. [ns]	11
Photocathode Material	Bialkali

Appendix C

Settings of the experimental setup.

Table C1: Settings of experimental setup for a beam profile measurement.

Type	**Value**
Voltage on C1 [V]	1333
Voltage on C2 [V]	1381
Voltage on C3 [V]	1388
Voltage on C4 [V]	1325
Probing interval	100 [ps]

Table C2: Settings of experimental setup for velocity measurement.

Type	**Value**
Voltage on C1 [V]	2400
Voltage on C2 [V]	2528
Voltage on C3 [V]	2400
Voltage on C4 [V]	2460
Probing interval	100 [ps]

Table C3: Settings of experimental setup for phantom measurement.

Type	**Value**
Voltage on C1 [V]	2199
Voltage on C2 [V]	2376
Voltage on C3 [V]	2203
Voltage on C4 [V]	2219
Threshold	110 [mV]
Trigger window	60 [ns]
Probing interval	100 [ps]

Appendix D

Charge spectra for all phantoms measurements before and after cut

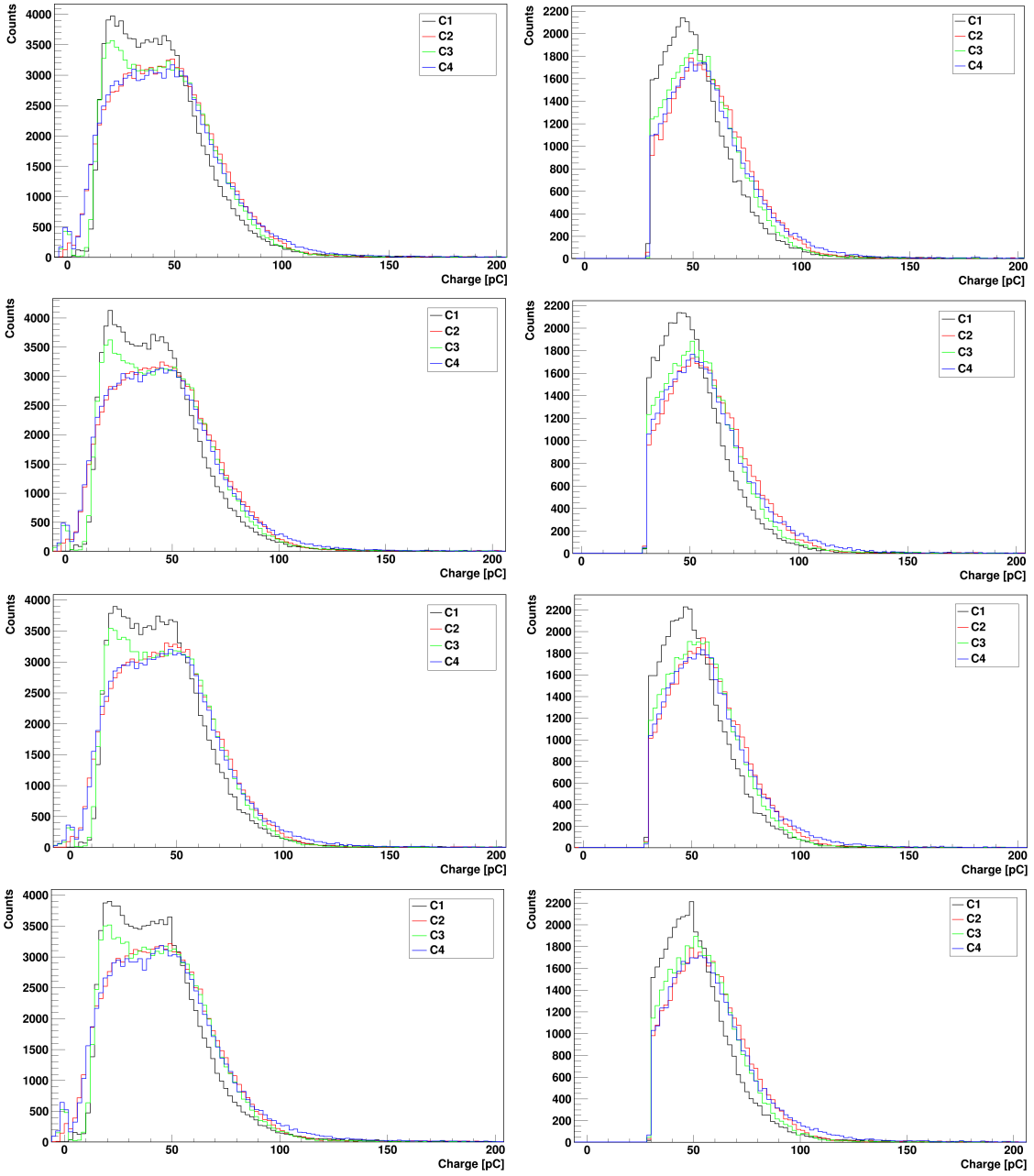

Figure D1: Charge spectra before (left) and after (right) cut for phantoms I - IV filled with water. The spectra are ordered in rows which number corresponds to the phantom number. From up to down (from I to IV).

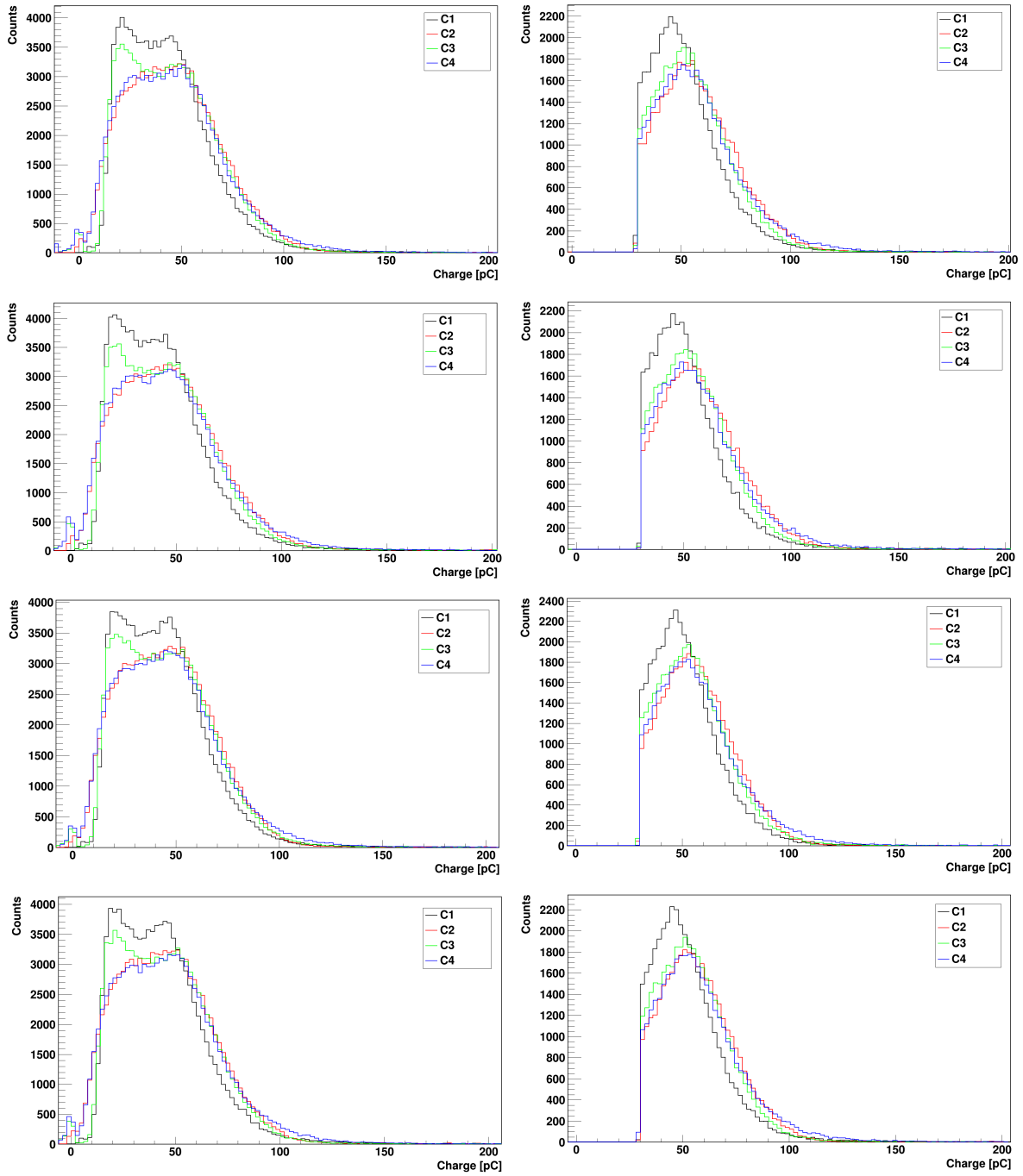

Figure D2: Charge spectra before (left) and after (right) cut for phantoms: I - IV filled with alcohol. The spectra are ordered in rows which number corresponds to the phantom number. From up to down (from I to IV).

Appendix E

Distribution of time difference between arrival of signals to opposite ends of the strip for all phantoms measurements

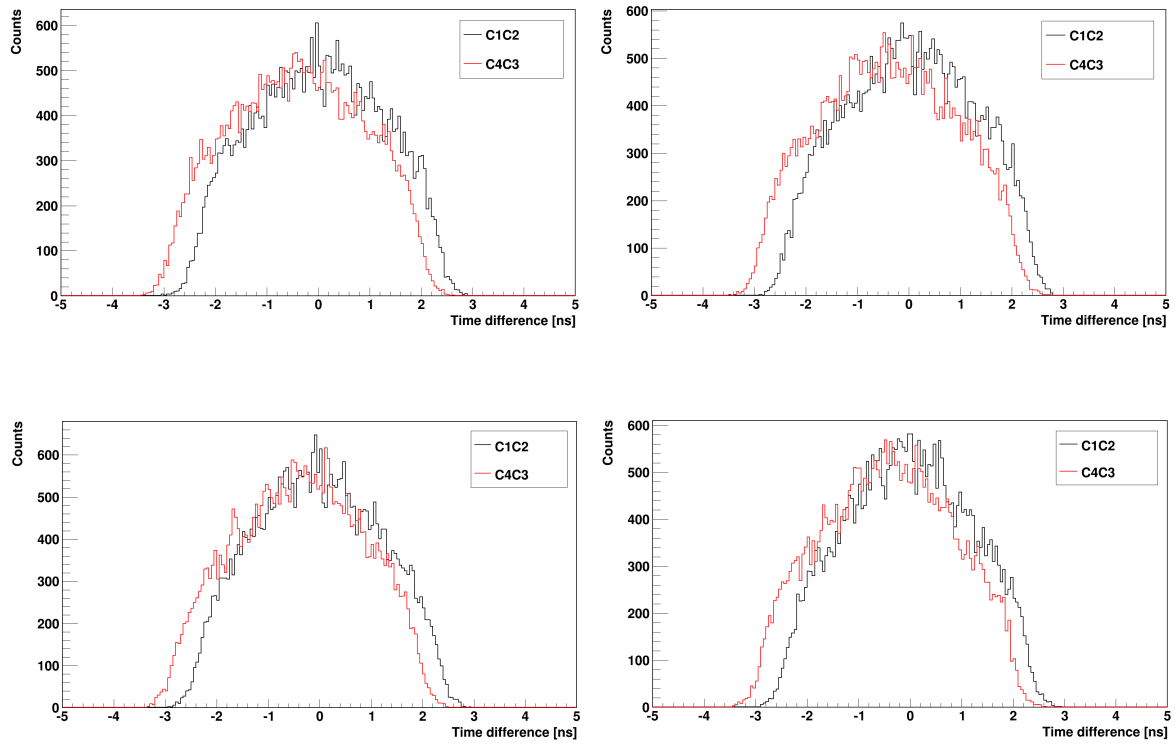

Figure E1: Distribution of time differences between arrival of signals to opposite ends of the strip for phantoms: I(top left), II (top right), III (bottom left), IV (bottom right) with water.

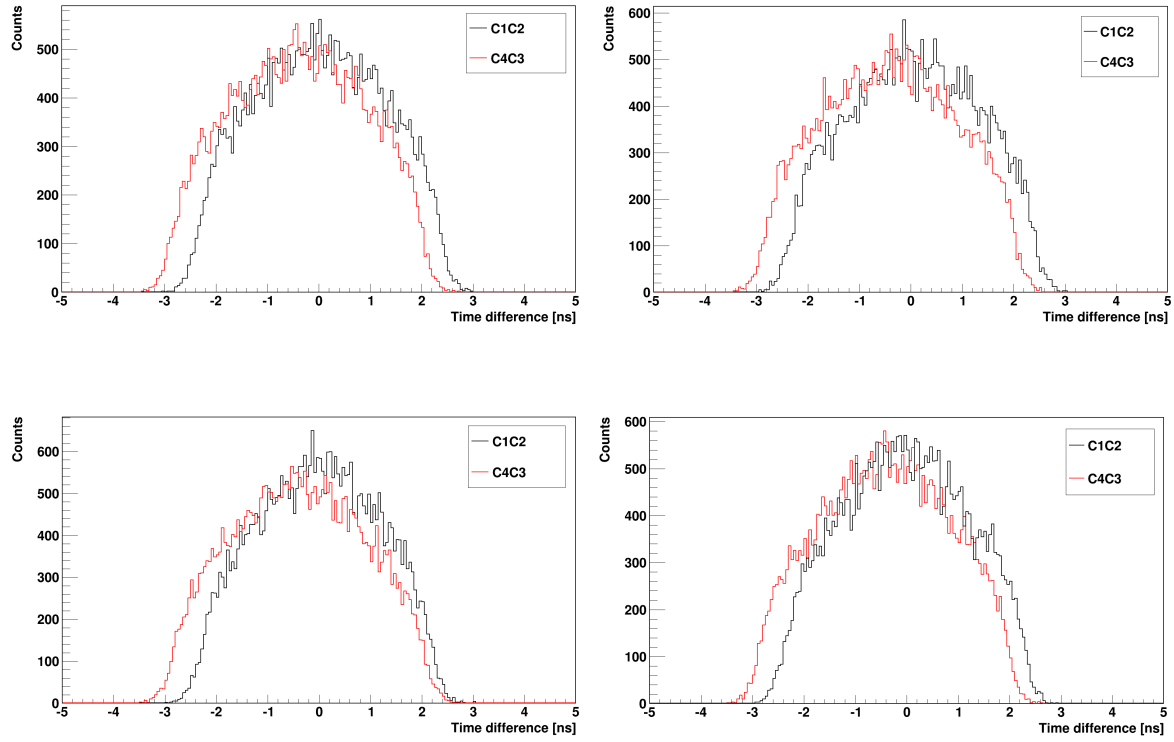

Figure E2: Distribution of time differences between arrival of signals to opposite ends of the strip for phantoms: I(top left), II (top right), III (bottom left), IV (bottom right) with alcohol.

Appendix G

Time-of-Flight resolution as a function of pairs of intervals for all phantoms measurements

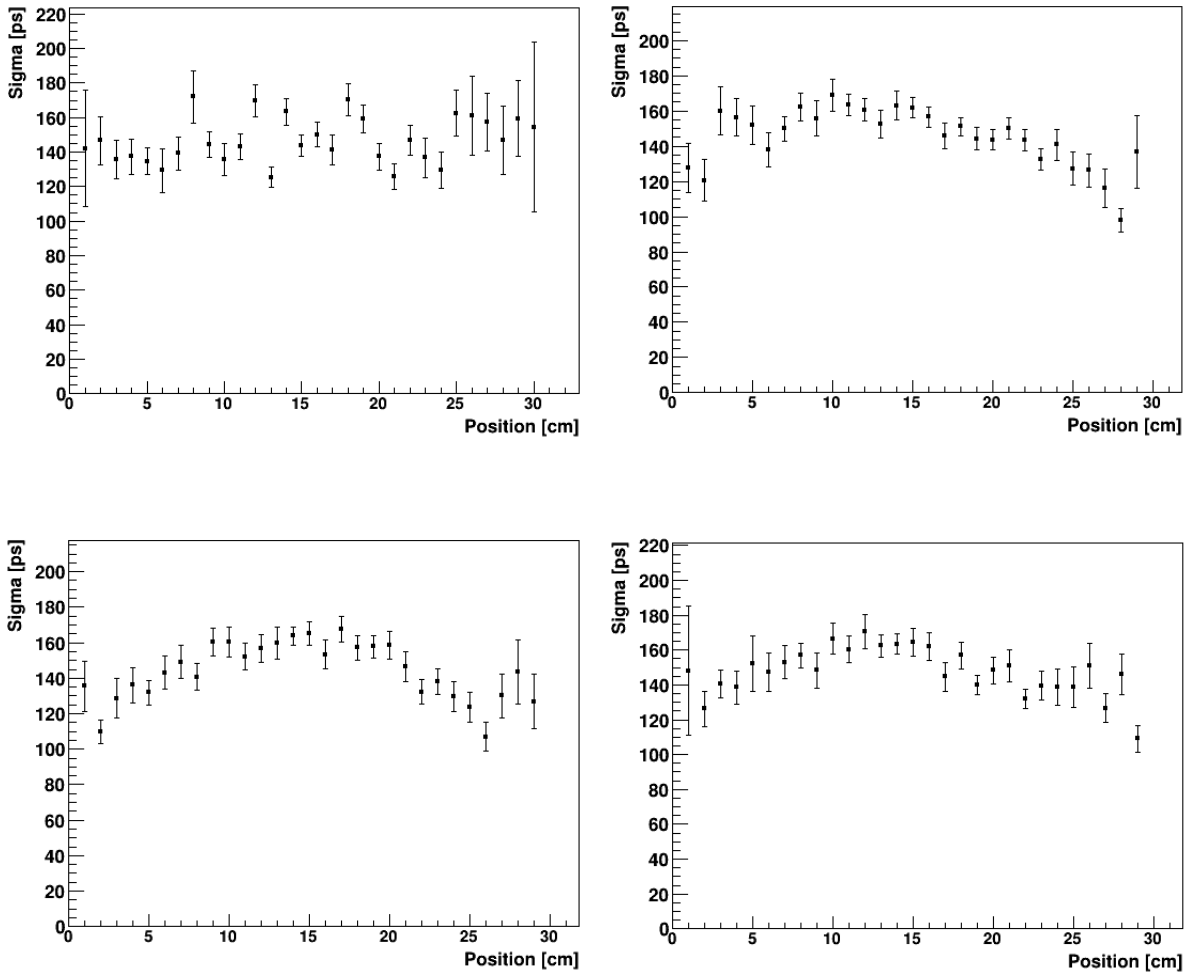

Figure G1: Time-of-Flight resolution as a function of position along the strip from both scintillators for phantoms: I(top left), II (top right), III (bottom left), IV (bottom right) with water.

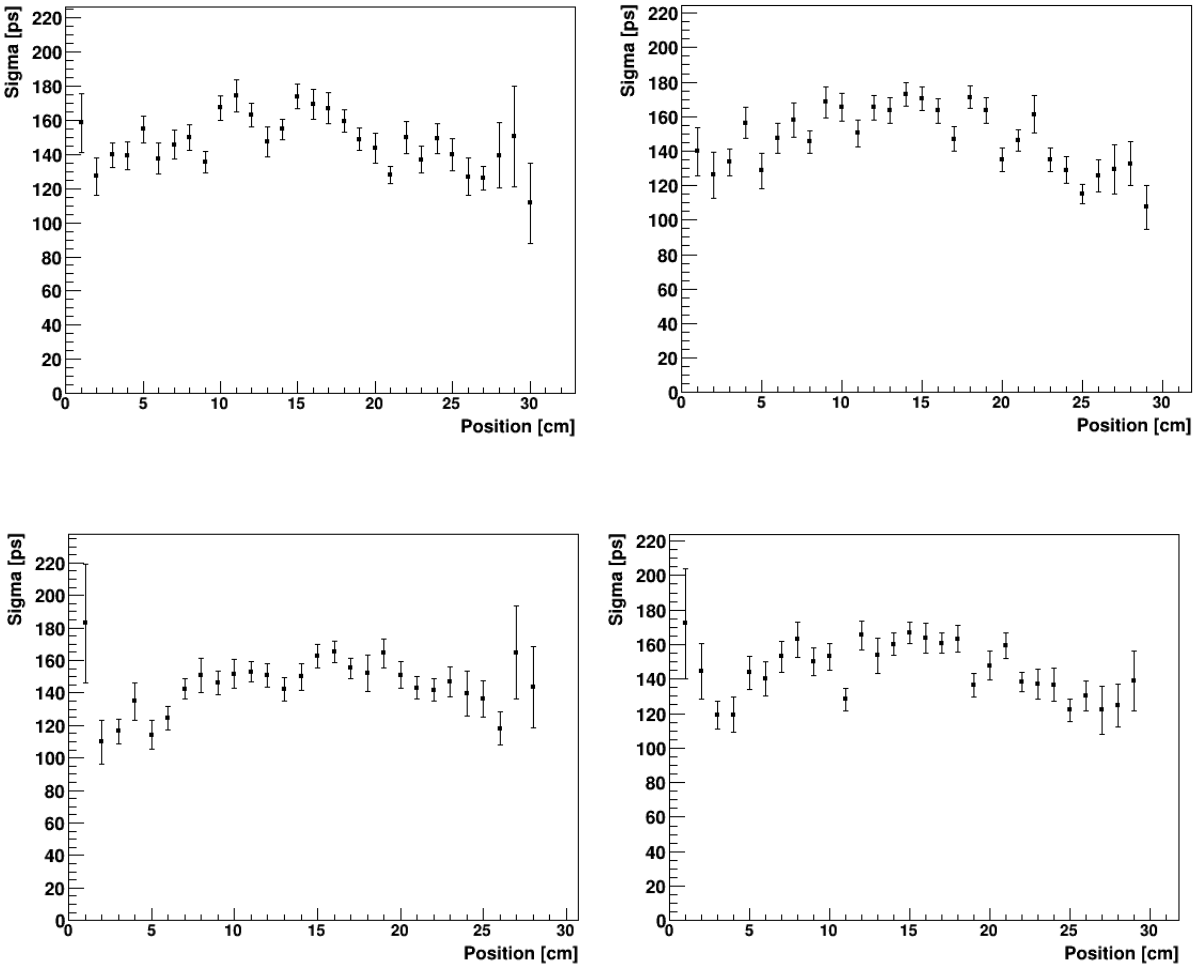

Figure G2: Time-of-Flight resolution as a function of position along the strip from both scintillators for phantoms: I(top left), II (top right), III (bottom left), IV (bottom right) with alcohol.

Appendix F

Time difference divided into 1 cm intervals in time domain of modules for all phantoms measurements

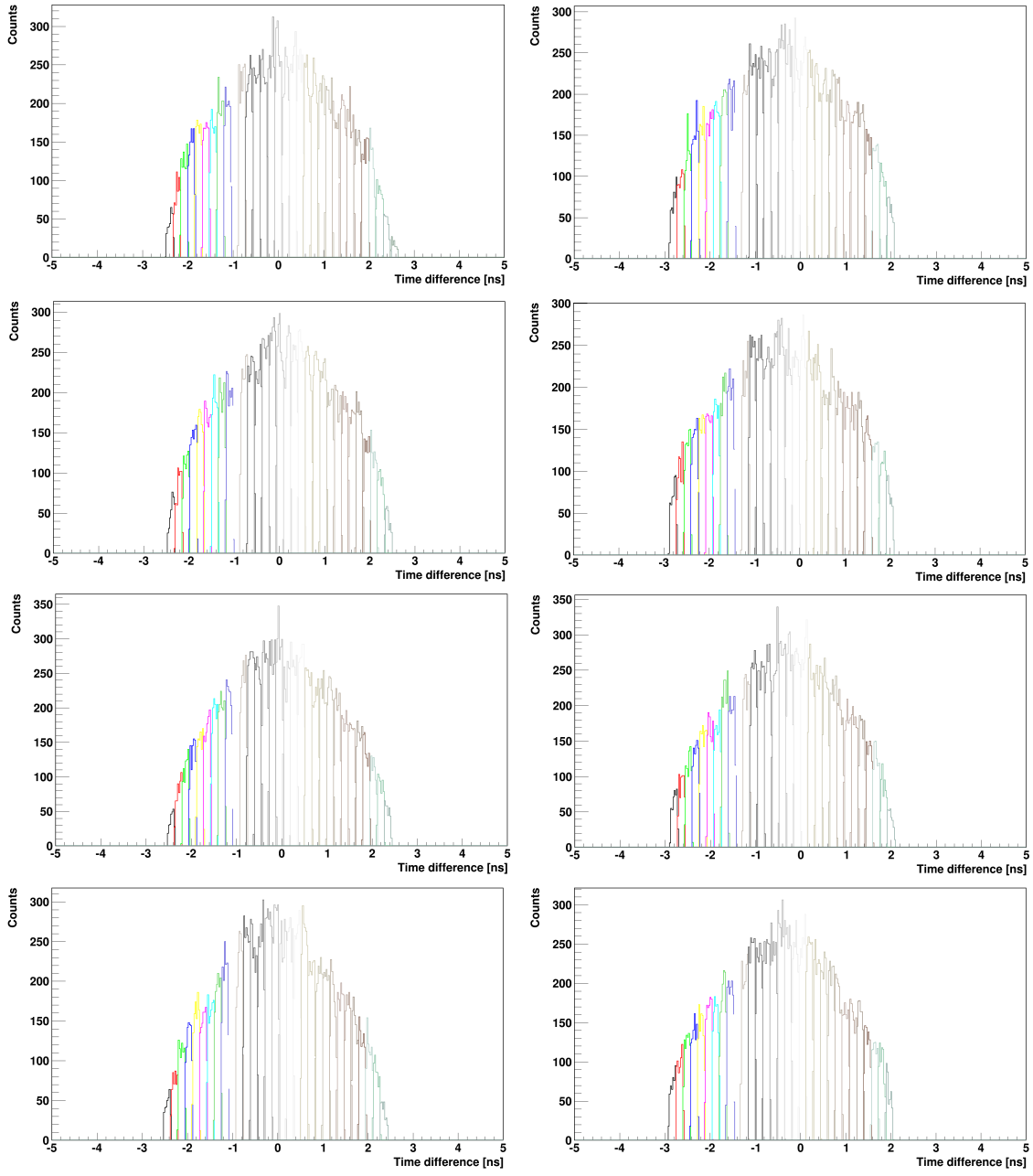

Figure F1: Distribution of time differences between arrival of signals to the opposite ends of the module C1C2 (left) and C4C3 (right) for phantoms filled with water. The spectra are ordered in rows which number corresponds to the phantom number. From up to down (from I to IV).

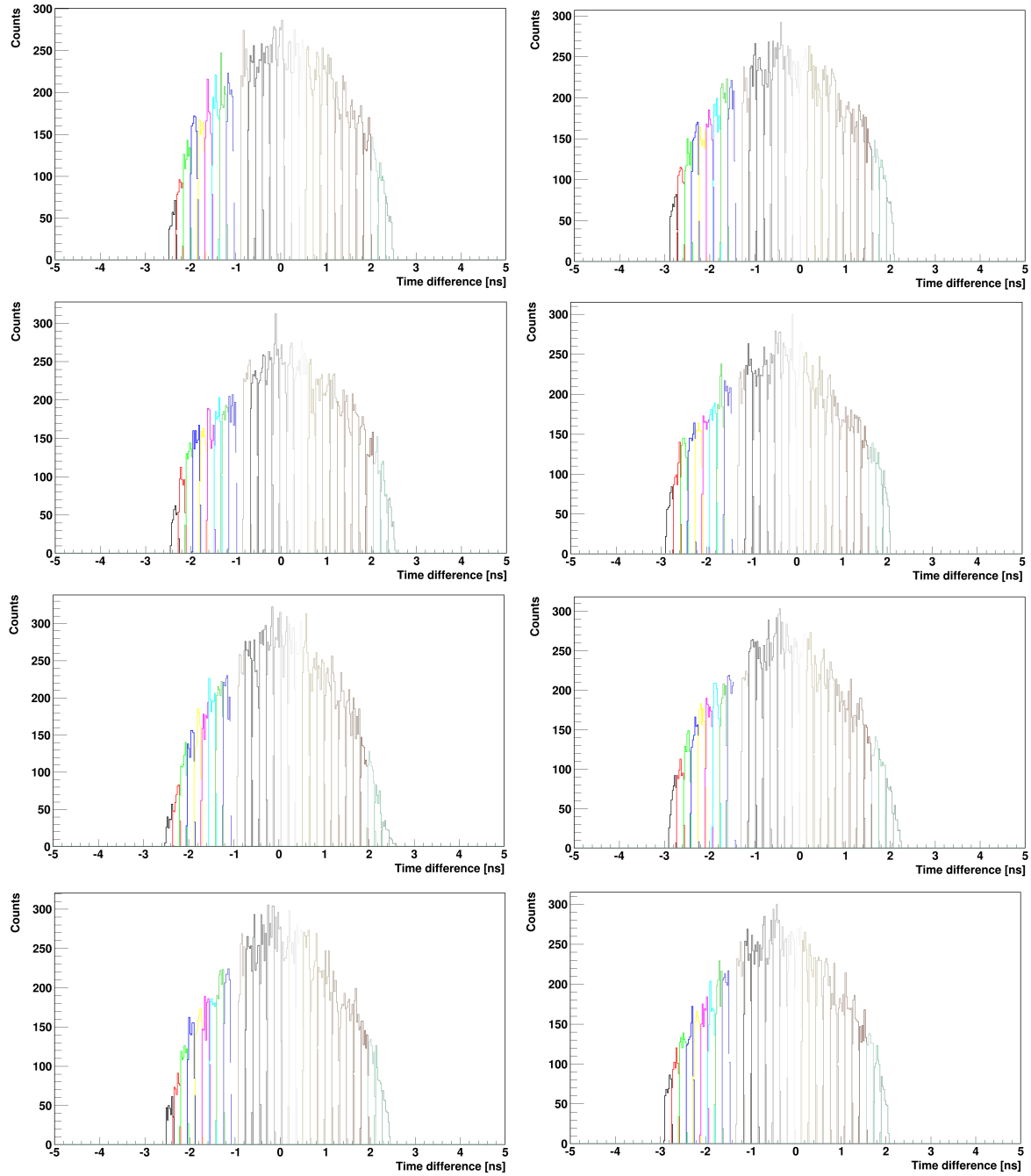

Figure F2: Distribution of time differences between arrival of signals to the opposite ends of the module C1C2 (left) and C4C3 (right) for phantoms filled with alcohol. The spectra are ordered in rows which number corresponds to the phantom number. From up to down (from I to IV).

References

[1] P. Moskal et al., *TOF-PET detector concept based on organic scintilators*, Nuclear Med. Rev. 2012: 15 Suppl. C: C81-C84.

[2] J. S. Karp, S. Surti, M. E. Daube-Witherspoon, G. Muehllehner, *Benefit of Time-of-Flight in PET: Experimental and Clinical Results*, J. Nucl. Med. 2008; 49:462.

[3] A. T. Nassalski, *Wspólny detektor do tomografii pozytonowej i rentgenowskiej*, PhD thesis (2010), The Andrzej Soltan Institute For Nuclear Studies.

[4] G. Saha, *Basics of PET imaging*. Springer, New York 2010.

[5] C. L. Melcher and J. S. Schweitzer, *Cerium doped lutetium oxyorthosilicate: A fast effcient new scintillator*, IEEE Trans. Nucl. Sci. Vol 39 (1992), 502-505.

[6] M. Conti, et al., *First experimental results of Time-of-Flight reconstruction on an LSO PET scanner*, Phys. Med. Biol. Vol. 50, 4507-4526 (2005).

[7] P. Moskal et al., Nuclear Inst. and Methods in Physics Research A 764 (2014), pp. 317-321

[8] M. Conti, *State of the art and challenges of Time-of-flight PET*, Physica Medica 2009; 25: 1-11.

[9] P. Moskal et al., *Strip-PET: a novel detector concept for the TOF-PET scanner*, Nuclear Med. Rev. 2012: 15 Suppl. C: C68-C69.

[10] P. Moskal, P. Salabura, M. Silarski, J. Smyrski, J. Zdebik, M. Zieliński, *Novel detector system for the positron emmision tomography*, Bio-Algorithms and Med-Systems 2011; 7:73-78.

[11] Z. Jaworski, *Dobroczynne promieniowanie*, Wiedza i Życie 1997; 3: 20-29.

[12] L. Dobrzyński, *Hormeza – Zjawiska powszechnie znane i nieznane*, *www.ipj.gov.pl/pl/szkolenia/matedu/hormeza.htm*.

[13] OIL Kielce, *http://www.nil.org.pl/xml/oil/oil56/gazeta/numery/n2007/n200705/n20070506*.

[14] W. W. Moses, Nuclear Medical Imaging-Techniques and Challenges, $http://instrumentationcolloquium.lbl.gov/Nuclear\%20Medical\%20Imaging.pdf$.

[15] D. R. Schaart, S. Seifert, R. Vinke et al., *LaBr3:Ce and SiPMs for TOF-PET: achieving 100ps coincidence resolving Time*, Phys. Med. Biol. 2010; 55:N179.

[16] R. Y. Zhu, *An LSO/LYSO Crystal Calorimeter for the ILC*, $http://www.slac.stanford.edu/econf/C0508141/proc/pres/ALCPG0705_TALK.PDF$

[17] R. Y. Zhu, D. Hitlin, *An LSO/LYSO Crystal Array for a Precision Lepton/Photon Detector at the ILC*, $www.pages.uoregon.edu/jimbrau/LC/lcdrd/abstracts06supp/hitlin-ILC\_fy07\_abs.pdf$

[18] J. L. Humm et al. *From PET detectors to PET scanners*, Eur. J. Nucl. Med. Mol. Imaging 2003; 30: 1574

[19] A. K. Buck, K. Herrmann, T. Stargardt, T. Dechow, B. J. Krause, J. Schreyögg, *Economic Evaluation of PET and PET/CT in Oncology*, J. Nucl. Med. 2010; 51: 401.

[20] Scintillation Products Data sheet, Saint-Gobain Ceramics & Plastics 2011.

[21] Sz. Niedźwiecki, *Studies of detection of gamma radiation by means of organic scintillator detectors in view of positron emission tomography*, Diploma Thesis 2011.

[22] V. Kouznetsov et al., *A large acceptance lead-scintillator Time-of-flight wall for neutral and charged particles*, Nuclear Instruments and Methods in Physics Research A 2002; 487: 396 – 406.

[23] Y. Schikaze et al., *Large-Area Scintillator Hodoscope with 50 ps Timing Resolution Onboard BESS*, Nucl. Instrum. Meth. 2000; A455: 596 - 606.

[24] G. Charpak, L. Dick, L. Feuvaris, *Location of the position of the particle trajectory in a scintillator*, Nuclear Instruments and Methods 1962; 15: 323 – 326.

[25] M. E. Werner, JS. Karp, *TOF-PET offset calibration from clinical data*, Phys Med. Biol. 2013; 21: 58(12)

[26] S. Surti, JS. Karp, *Experimental evaluation of a simple lesion detection task with Time-of-Flight PET*, Phys. Med. Biol. 2009 January 21; 54(2): 373–384.

[27] C. Lois et al., *An Assessment of the Impact of Incorporating Time-of-Flight (TOF) Information Into Clinical PET/CT Imaging*, J. Nucl. Med. 2010; 51(2): 237.

[28] S. Surti et al., *Impact of TOF-PET on whole-body oncologic studies: a human observer lesion detection and localization study*, J. Nucl. Med. 2011; 52(5): 712–719.

[29] D.J Kadrams et al., *Impact of Time-of-Flight on PET Tumor Detection*, J. Nucl. Med. 2009; 50(8): 1315–1323.

[30] M. B. Daube-Witherspoon et al., *Imaging performance of a LaBr3-based PET scanner*, Phys. Med. Biol. 2010; 55(1): 45–64.

[31] M. S. Tohme, J. Qi, *Iterative Image Reconstruction for Positron Emission Tomography Based on Detector Response Function Estimated from Point Source Measurements*, Phys. Med Biol. 2009 June 21; 54(12): 3709–3725.

[32] Scintillator Products, Saint-Gobain Ceramics & Plastics (2009).

[33] J. T. M . de Hass, P .Dorenbos, *Advances in yield calibration of scintillators*, IEEE Trans. Nucl. Sci. Vol. 55 (2008), 1086-92.

[34] S. Usuda, et al., *Phoswich detectors combining doubly or triply ZnS(Ag), NE102A, BGO and/or NAI(Tl) scintillators for simultaneous counting of , and rays*, Nuclear Instruments and Methods in Physics Research Vol. A 340 (1994), 540-545.

[35] *www.hamamatsu.com/us/en/R4998.html*

[36] *www.hamamatsu.com/us/en/R9800.html*